**Master of Science**

# Synthesis of N doped $Cu_3Mo_2O_9$

# as a bifunctional electrocatalyst for water splitting

The Graduate School of the University of Ulsan

Department of Chemical Engineering

Huynh Ngoc Khanh

# Synthesis of N doped $Cu_3Mo_2O_9$

# as a bifunctional electrocatalyst for water splitting

Supervisor: Professor Choi Won Mook

A Dissertation

Submitted to

The Graduate School of the University of Ulsan

In Partial Fulfillment of the Requirements for the Degree of

Master of Science

By

Huynh Ngoc Khanh

Department of Chemical Engineering

University of Ulsan, Korea

August 2023

# Synthesis of N doped $Cu_3Mo_2O_9$

# as a bifunctional electrocatalyst for water splitting

This certifies that the master's thesis of Huynh Ngoc Khanh is approved

_____

Committee Chair Prof. Sung Gu Kang

_____

Committee member Prof. Won Mook Choi

_____

Committee member Prof. Eun Woo Shin

Department of Chemical Engineering

University of Ulsan, Korea

August 2023

# Table of contents

# Acknowledgement

This researches cannot complete without the support of Professor Won Mook Choi and Dr Tran Van Tam who teach, give me advise during my master program. In Here I would like to express my gratitude to them

I also would like to thank Dr Tata Sanjay Kanna Sharma and my labmates Beena Mol Babu, Srushtee Sanjay Bhosale and Kim MinJi to help me in work

I really respect all of my friends who beside me during master program to help me improve my knowledge and skill for better performance in work

I am extremely thankful to all members University of Ulsan for valuable opportunities to study condition

# List of tables

# List of figures

# Summary

The content of this thesis includes 2 main parts

Chapter 1 illustrates water splitting reaction. firstly, the overview is about energy consumption and the pressure to environment, the development of economics of many countries which causes by using and exploiting natural resources for energy demand. Then, hydrogen energy becomes potential candidate to replace fossil fuels. Next, theory about water splitting is mentioned. Besides, some catalyst concepts can be understood due to principle of the reaction. Finally, this chapter also give information about popular parameters to evaluate electrocatalyst

In chapter 2, basing on the necessity of water splitting process, the electrocatalyst for water splitting is studied. This part supports the explanation about composite design. Secondly, the practical methods to synthesize material is describes. Analytical measurements to understand the composite and to confirm the efficiency of catalyst for water splitting are also researched. After that, the result is recorded to analysis and compare with commercial product

# Chapter 1 : Introduction

## 1.1 Background

Energy is essential demand of human in modern life. Energy exhibits its important role not only in daily but also in industrial environment. Besides, it is evaluated that energy is factor which affect the development of economics and social all over the world[1]. Traditionally, fossil fuel (coal, oil and natural gas) is mostly used in energy production process. However, this kind of material has many problems. The significant grow up of population lead to the dramatically increase of energy consumption. From this, fossil fuel express disadvantages clearly[2]

Fossil fuels causes strongly negative influence on environment. After undergoing combustion process, fossil fuels emit CO2, pollutant, greenhouse gas. Moreover, acid rain and global warming is believed to be the effect of fossil fuel combustion. These environment phenomena occur for a long time can lead to the consequence of heavy natural disaster and human health threaten[1,3]. Data of International Energy Agency (IEA) reports the amount CO2gasfrom 2000 to 2022. Three clearly reasons for CO2 releasing are coal, oil and natural gas with 1.5 GtCO2eq, 11.2 GtCO2eq and 7.3 GtCO2 eq respectively (GtCO2 eq: gigatons of CO2 equivalent). As can be seen, CO2 emission more and more increase year by year. And this trend still continuously increases several ye Fossil fuel has influence on many aspects of society especially economic of country. Fossil fuel can be known as type of natural resources so the amount of this sources is limit. Furthermore, not anywhere has fossil fuel[4]. Due to these properties, fossil fuel price depends on politics, strategies of countries and so on. The illustrated graph below of IEA indicates fossil fuel consumption subsidies by fuel from 2010 to 2022. In 2022, the crisis about fossil fuel price affects many countries. The Subsides worldwide increase significantly up to 698 billion for oil, natural gas and are after if solution

could not be suggested coal in 2022. The price of fossil fuel rose rapidly which strongly impact industrial environment and daily life[5]

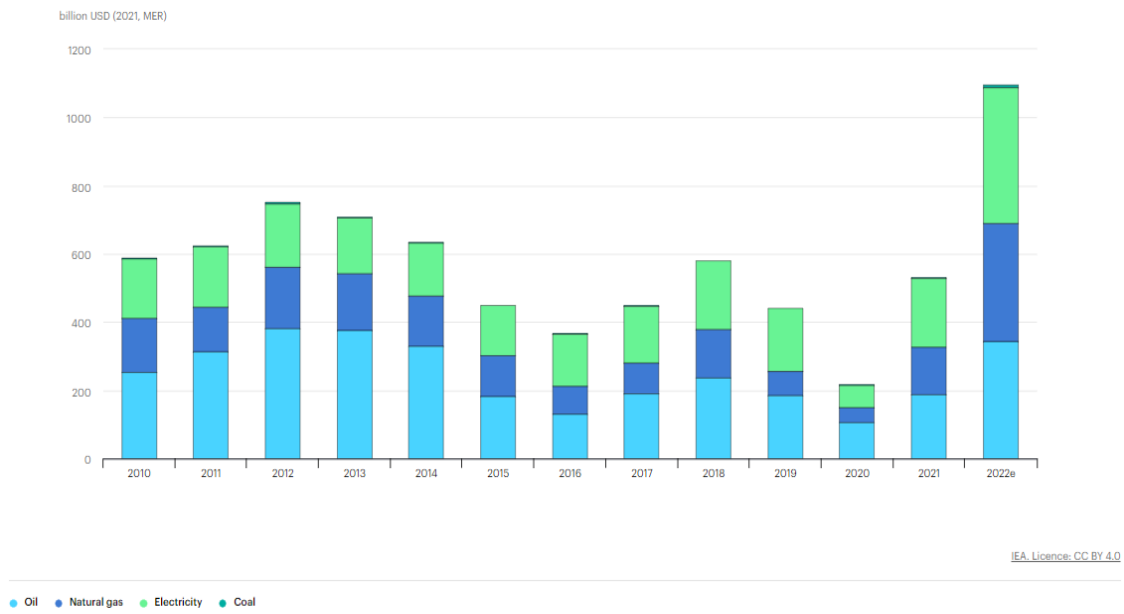


Figure 1.1: Fossil fuel consumption subsidies by fuel from 2010 to 2022[5]

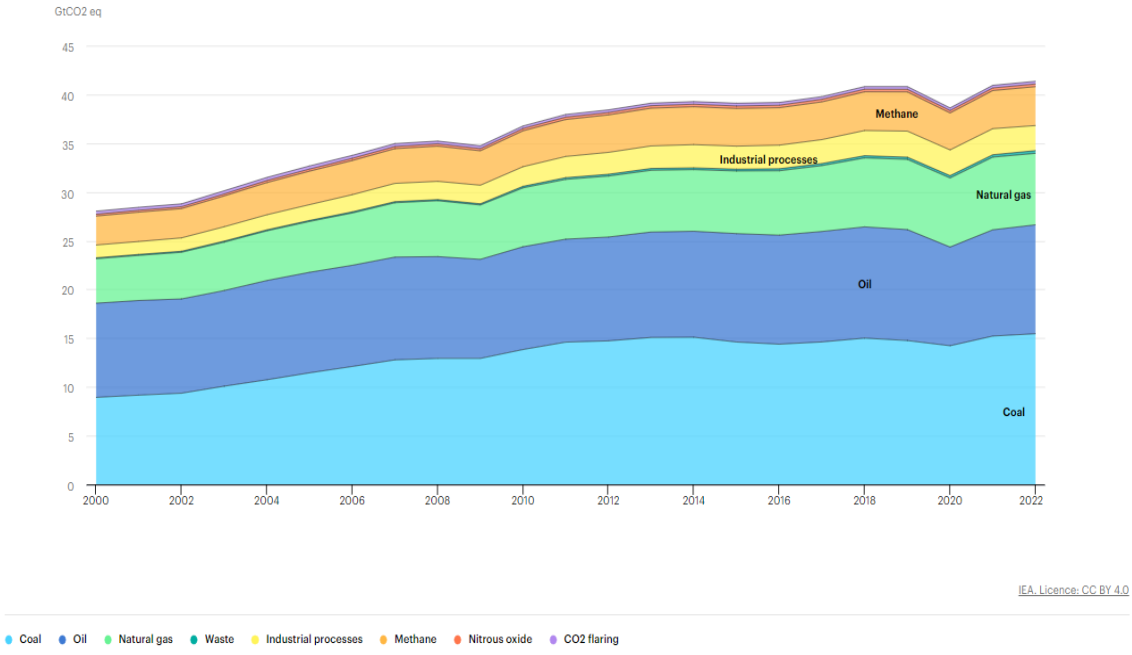


Figure 1.2: Global energy- related greenhouse gas emission from 2000 to 2022[4]

Facing to a lot of problems, the demand of energy still increases day by day. The renewable resources (wind, solar, geothermal and so on) are potential competitor to solve these problems[6]. However mentioned sources do not have reasonable storage and transfer method. Hydrogen is recommended to solve difficulties. With high energy density, Hydrogen is easily to storage and moving.[7]

1.2 Water splitting

Water splitting is an electrochemical reaction to separate water into Hydrogen and Oxygen. Basing on this proceed, Hydrogen fuels are environment friendly produce. In electrochemistry, water splitting divides into 2 half reaction which are call Hydrogen evolution reaction (HER) and Oxygen evolution reaction (OER). Reduction process will happen and produce oxygen at anode while oxidation produces Hydrogen at cathode. Water splitting is normally study in 2 environments: acidic and base. In theory, 1.23V is the necessary for water splitting to start. However, HER and OER practically require large overpotential so that water splitting need to applied potential lager than 1.23V[8–10]

**Total reaction:**

$2H_2O \rightarrow H_2+O_2$ E0=-1.23V

**In acidic condition**

$2H_2O \rightarrow O_2+4H^+ +4e^-$ E0=-1.23 V

$4H+4e^- \rightarrow 2H_2$ E0=0.00V

**In alkaline solution**

$4OH^- \rightarrow O_2+H_2O+4e^-$ E0=-0.40V

$4H_2O+4e^- \rightarrow 2H_2+4OH^-$ E0=-0.83V

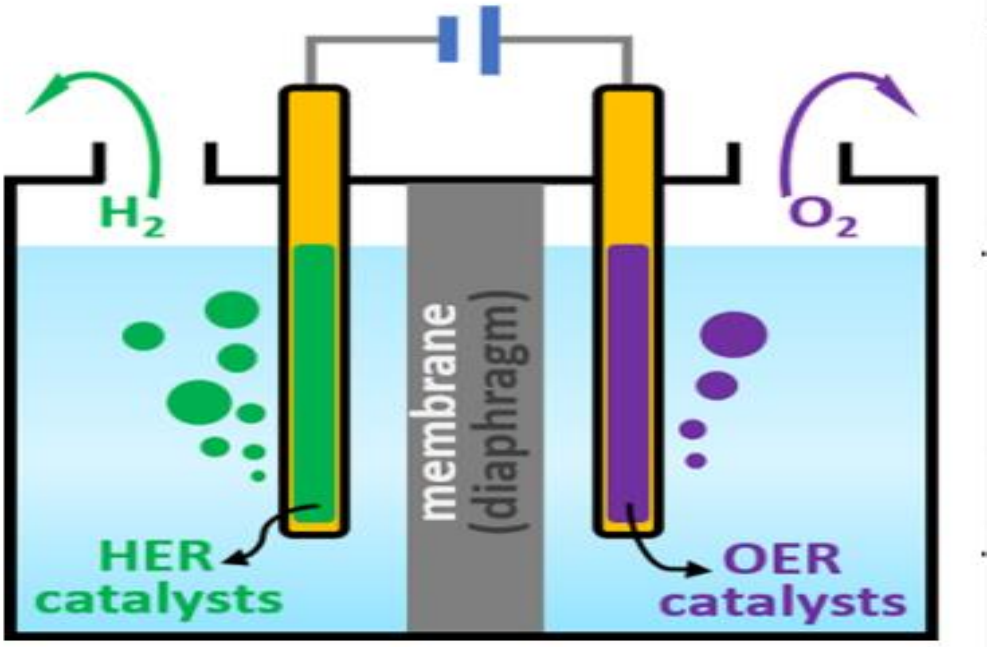


Figure 1.3: water splitting illustration[6]

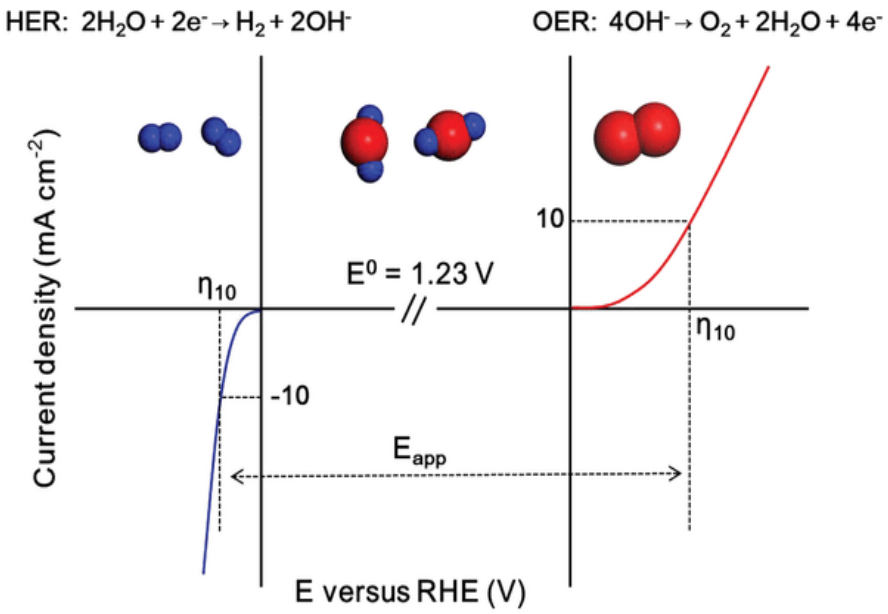


Figure1.4: Overpotential in water splitting[12]

Hydrogen evolution reaction (HER)

In various electrolyte, HER has different equation. In acidic medium, catalyst surface catches protons of Hydronium cation (H3O+) by electron lead to Hydrogen atom will be adsorbed by catalyst (H*) (Volmer reaction). Then adsorbed hydrogen, electron and proton combine to create Hydrogen (Heyrovsky reaction). Two adsorbed Hydrogen can couple with each other to generate hydrogen (Tafel). HER in base medium also have 3 types equations. To from adsorbed Hydrogen, catalyst catches proton from H2O and electron (Volmer reaction). In next step, H2O molecule continuously couples with adsorbed Hydrogen together with electron to give hydrogen (Heyrovsky reaction). Tafel step in alkaline condition is similar to in acidic environment [6,11–13]

| | acid | alkaline |
|---|---|---|
| Volmer | $H_3O^+ + e^- + * \rightarrow H^* + H_2O$ | $H_2O + e^- + * \rightarrow H^* + OH^-$ |
| Heyrovsky | $H^* + H_3O^+ + e^- \rightarrow H_2 + H_2$ | $H^* + H_2O + e^- \rightarrow H_2 + OH^-$ |
| Tafel | $H^* + H^* \rightarrow H_2$ | |

Table 1.1: HER equation in acidic and base condition

Alkaline electrolyte is popular to apply for HER in industry. In acidic condition, there is great source H to support H* for HER but in alkaline medium, H* formation occurs due to water dissociation. HER in base environment is affected by water dissociation which lead to sluggish kinetics of reaction. Free energy of adsorbed hydrogen ($\Delta G_{H^*}$) is also important to HER. Ideal $\Delta G_{H^*}$ for a catalyst should be nearly 0. With too weak free energy, it causes difficulty in proton and catalyst surface interaction while too strong $\Delta G_{H^*}$hinders hydrogen to release from catalyst[11–13,14]

Electrocatalyst for HER is designed to adapt 2 essential aims: (1) supporting water dissociation, (2) optimize free energy of hydrogen. These 2 purposes limits input energy to drive the reaction

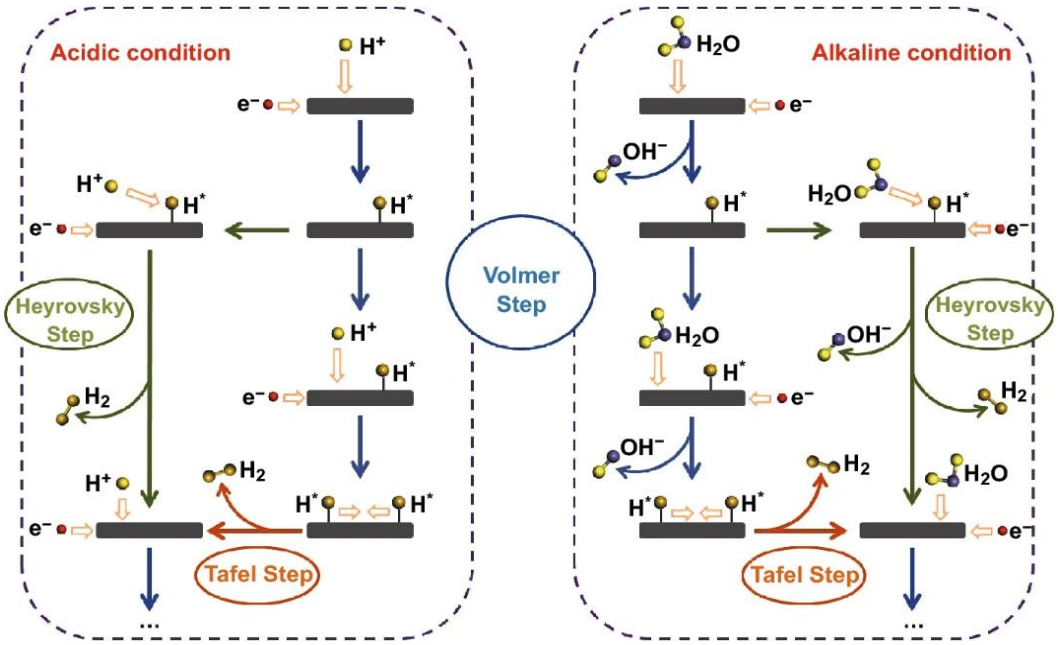


Figure 1.5: HER mechanism[11]

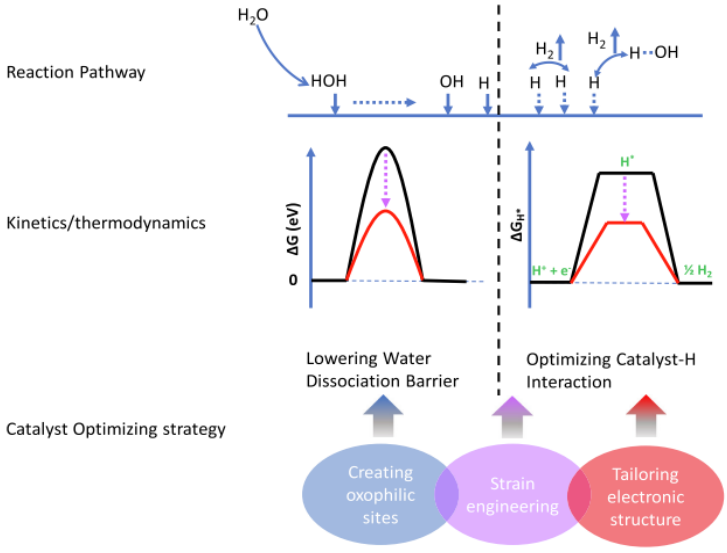


Figure1.6: HER electrocatalyst concept[12]

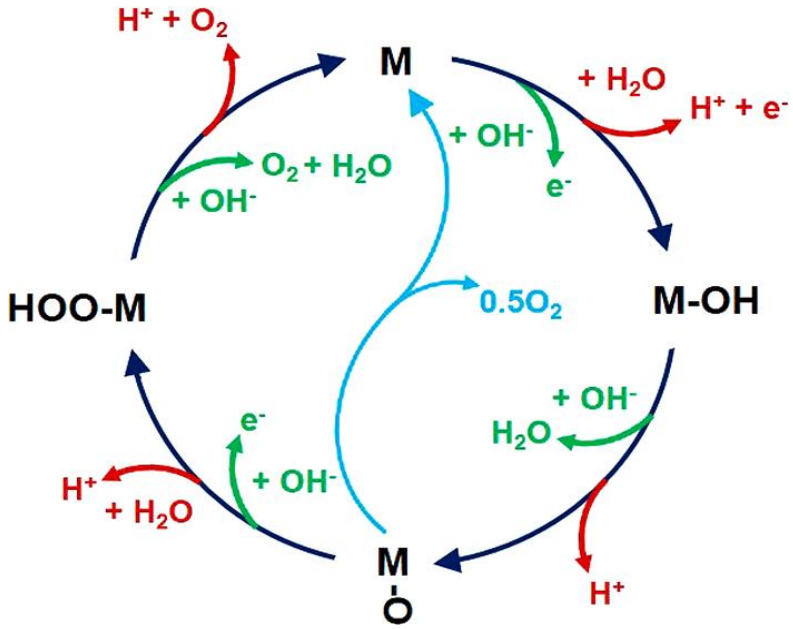


Figure 1.7: OER mechanism[14]

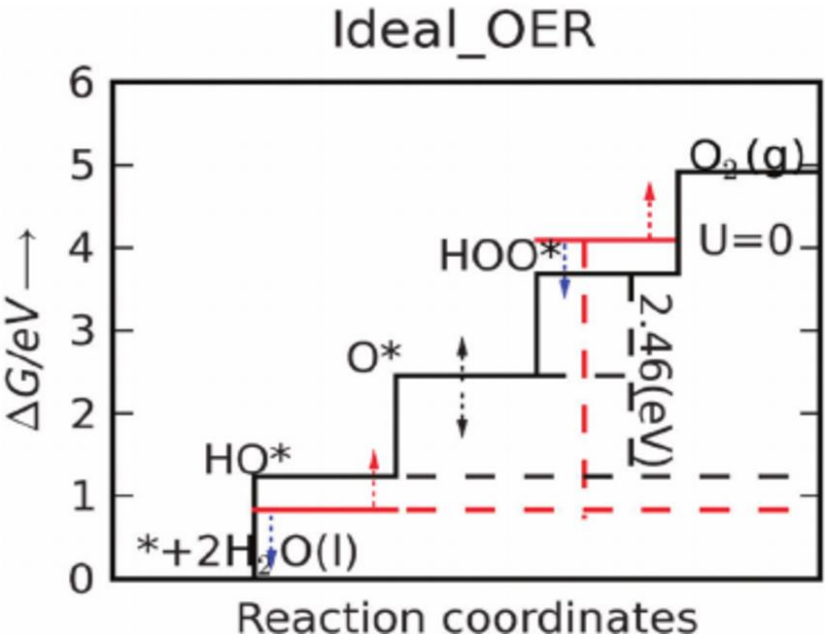


Figure 1.8: OER energy description[16]

The catalyst concept can improve by electronic structure technique, strain engineering or creating oxophillic sites. Besides, another factor also impacts HER efficiency is active area and conductivity of composites[12]

1.2.1 Oxygen evolution reaction (OER)

OER is more complicated than HER. In acidic medium, $H_2O$ molecule decomposes to Oxygen and hydrogen ions while hydroxyl ion divides into water and oxygen in base environment. Normally in OER process, OH*, O* and OOH* is essential component which are adsorbed on catalyst material. OER mechanism can be summarized in 3 main steps.Catalyst captures Hydroxyl or H2O then coupled proton and electron transfer occurs. Finally, oxygen molecule is formed and release to electrolyte. During OER process, there are four steps which transfer electron and proton.[15–18]

In equilibrium state, Free gibs energy of OER ($\Delta G_{OER}$) is 1.23V for each step which is the ideal condition. Practically, OER still requires energy because the limitation speed of the OER causes by step which has highest ΔG value. The different free energy value of OH* and OOH* can be studied through constant value 3.2eV (2.46eV in ideal condition)

| **Acidic medium** | **Alkaline medium** |
|---|---|
| $H_2O+*\rightarrow OH*+H^++e^-$ | $OH^-\rightarrow OH*+e^-$ |
| $HO*\rightarrow O*+H^++e-$ | $HO*+ HO*\rightarrow O*+H_2O+e-$ |
| $O*+H_2O\rightarrow HOO*+H^++e^-$ | $O*+OH^-\rightarrow HOO*+e^-$ |
| $HOO*\rightarrow *+O_2+H^++e^-$ | $HOO*\rightarrow *+O_2+ H_2O +e^-$ |

Table 1.2: OER equation in acidic and base condition

1.2.2 Electrocatalyst evaluation parameter

**Overpotential** [10,19]

The variance between equilibrium potential and the practical potential at definite current when the reaction occurs with catalyst is overpotential ($\eta$). Overpotential is unexpected value when evaluating a catalyst for a reaction. High overpotential records which means high input energy require to drive the reaction. Practically, overpotential data at specific current density can be collected from Linear swept voltammetry LSV measurement. Additionally, Overpotential at current density of 10 $mA/cm^2$ is popular value to compare and evaluate sample activity

$$E_{electrolysis} = IR + E_{reversible} + \Delta E_{irreversible}$$

Where

IR: the drop in voltage

$E_{reversible}$: the theorical decomposition voltage

$\Delta E_{irreversible}$: overpotential of OER

**Tafel slope and exchange current density**[2,10,19,20]

**Tafel slope** described reaction kinetic. Tafel slope is linear plots of overpotential and current density log (i). The lower Tafel slope is, the faster reaction occurs and reversibly. Tafel equation can be applied for both 2 half reaction of water splitting HER and OER. Practically, Tafel slope value can be archived form LSV measurement

$$\eta = a + b\log(i)$$

Where

$\eta$ : overpotential

a: intercept relative to the exchange current density

b: Tafel slope (mV $dec^{-1}$)

i: current density ($mA^{-2}$)

Exchange current density ($i_0$) is known as the current of the system at point $\eta$=0 without net electrolysis. This parameter exhibits how kinetic of electron transfer at equilibrium point. $I_0$ can be derive from Tafel equation

**Electrochemical Impedance Spectroscopy (EIS)**

EIS measurement gives charge transfer resistances (Rct) which poses electrode kinetic. Electrocatalyst with high charge transfer resistances means it hinders electron to transfer and the reaction occurs slowly

**Stability**

Stability is one of the essential criteria to prove that electrode catalyst can stand reaction condition for a long time. For stability, 2 types of measurement can be used. The first one is stability of catalyst after many cyclic voltammetry (CV) circles. The catalyst undergoes CV circles then Linear sweep voltammetry (LSV) is recorded. LSV data after test is compared with the LSV data before stability test. The second types of stability test include 2 optional measurements: chronopotentiometry (CP) or chronoamperometry (CA). for CA, the constant potential is applied to the system and the current is recorded over long times. In this study, CP is measures to evaluate stability. The potential of electrode following time is given whilethe constant current is controlled for the system.

**Mass and specific activity**

Mass activity is parameter which evaluates performance of catalyst base on the material mass loading (unit: A/g). The great mass activity value can represent for good electrocatalyst. Specific activity indicates activity of catalyst through Electrochemical surface area (ECSA). ECSA give information about active site of the material which is important to an electrocatalyst. The more active site catalyst has, the more convenient water molecule adsorption and intermediate adsorption are. It can be understood that large ECSA is advantage in electrocatalyst of water splitting [21–23]

# Chapter 2 : Synthesis of N doped $Cu_3Mo_2O_9$/NF for high efficiency electrocatalyst of water splitting

ABSTRACT

Due to highly desired green energy demand, developing high performance and stable materials for catalyzing in water electrolysis is essential yet challenging. Besides, affordable and binder-free catalyst growth on Ni foam is one of the most important criteria to evaluate industrial application. Herein, Nitrogen doped $Cu_3Mo_2O_9$ (N-$Cu_3Mo_2O_9$) which is growth directly on Nickel foam, is demonstrated as efficient catalyst for water splitting. The material is synthesized in 2 main step hydrothermal and calcination. Analytical result indicated that the material covers the surface of the Nickel foam to create the porous structure that leads to high surface area for the composite. Electrochemical performance shows remarkable activity with small overpotential value at current density of 10 mA/cm$^2$ for hydrogen evolution reaction (HER, $\eta 10$ =30 mV) and Oxygen evolution reaction (OER, $\eta 10$ =180 mV), respectively. The excellent HER and OER stability of the material are evaluated at high current density of 100 mA/cm$^2$ which maintain over 90% after 30 hours, outperforming commercial material under the same condition. Interestingly, the N-$Cu_3Mo_2O_9$-based electrolyzer was constructed and possessed good catalytic activity toward water slitting driven by solar cell.

## 2.1 Introduction.

In recent decade, environment problems and scary of fossil fuel have been attracted a huge attention not only in industry but also academic. The demand of energy climbs tremendously leads to strongly attraction of pollution and economics issues. Undergoing combustion process, fossil fuel release big amount of $CO_2$[2,3,5]. In this case, Hydrogen is paid attention as promising candidate to replace fossil fuel which is green and sustainable sources for energy produce[7,24]. Hydrogen can be produced by many technique, water splitting is one of highly recommendatory methods because of its simply and efficiency[24]. However, the current water splitting system is inhibited owing to sluggish kinetic of its two half-reactions: Hydrogen evolution reaction (HER) and Oxygen evolution reaction (OER)[11,25,26]. Until now, some materials as $IrO_2$, $RuO_2$, Pt/C and so on perfume excellent catalyst role. However, they still have some defect about uneconomic and unstable characteristic that encourage the exploration of new generation catalyst [9,18,20,27–30].

Due to multi-valance states and electronic structure, transition metal is used widely in electrochemical application. Additionally, affordability and good physical properties of transition metal make this material become promising candidate to replace noble metal as Ir, Pt, Pd, Ru[19,23]. Nitrogen-transition metal bond forms and leads to change in electronic structure of both Nitrogen and transition metal[31,32].

Water dissociation[13] and OH* are reasons which make reaction require much energy. One of suggested solution is to combine material with an oxophilic factors. In this situation, Molybdenum is chosen as an oxophilic metal. Molybdenum is affordable sources with a natural abundance. Additionally, benefit of Molybdenum is not only strong absorption OH but also its corrosion strength and high melting temperature[33]. Then, Nitrogen and copper combination lead to the changing in electronic structure as mention before which improve HER performance of material[31].

Here in, Nitrogen doped $Cu_3Mo_2O_9$ is built directly on Nickel foam where porous structure formed (7N-$Cu_3Mo_2O_9$). The synthesis method includes 2 main steps: hydrothermal and anneal. The excited activity of composite is indicated according to following data. In the alkaline environment 1,0M KOH at 30ºC, the onset potential of HER is12mV and this value of OER is 1360mV.When energy is applied, the overpotential of HER and OER are 30mV and 180mV at current density of 10 mA $cm^{-2}$ respectively. For comparison, Pt/C (20 wt%) and $IrO_2$ are commercial material used in similar condition and it indicates that in overall water splitting 7N-Cu3Mo2O9 is better performance according tostability in 80 hours at 100mA$cm^{-2}$ which decreases about 4.2% while commercial drops around 5.5%

2.2 Experimental

**Materials**

Nickel foam (NF), Ethylene glycol, ethanol, polyvinylpyrrolidone ($(C_6H_9NO)_n$), potassium hydroxide, flake (KOH), Urea, Copper (II) nitrate trihydrate ($Cu(NO_3)_2.3H_2O$), Sodium Molybdate (VI) dihydrate ($Na_2MoO_4.2H_2O$) were used as received without any further purification from Sigma-Aldrich. Deionized water (DI) produced by a Milli-Q Millipore system (18.2 MΩ, Millipore Corp, Billerica, MA) was used in all the experiments.

**Synthesis method**

Synthesis of N-$Cu_3Mo_2O_9$/NF

The NF was washed with ethanol in ultrasonic bath in 30 minutes and then dried in the oven at 60ºC overnight. Then, $Cu(NO_3)_2.3H_2O$, $Na_2MoO_4.2H_2O$ with the weight ratio 1:1 were added into 30µl ethylene glycol. PVP powder was added into the mixture with the concentration 0.09 mg/µl. The mixture was sonicated in 30 minute and transferred to 50 ml autoclave .NF was also put into autoclave. During hydrothermal process, autoclave was treated under condition of $180^{O}C$ in 12 hours. After Hydrothermal step, the NF was washed slightly with water and dried in the oven. Then Urea in ethanol solution was dropping on the surface of the NF with the existence of drying machine. Finally,

NF was annealed at 600°C in 2 hours. The sample with 0%, 3%, 5% and 7% weight Urea was named $Cu_3Mo_2O_9$, 3N-$Cu_3Mo_2O_9$, 5N-$Cu_3Mo_2O_9$ and 7N-$Cu_3Mo_2O_9$ respectively

Synthesis of Gly-Cu3$Mo_2O_9$/NF, PVP-$Cu_3Mo_2O_9$/NF and A-$Cu_3Mo_2O_9$/NF

For evaluating effect of ethylene glycol and PVP, Gly-$Cu_3Mo_2O_9$/NF was prepared without PVP, while PVP-$Cu_3Mo_2O_9$/NF was synthesized without Ethylene glycol. A-$Cu_3Mo_2O_9$/NF was formed without PVP and without ethylene glycol. All above samples were prepared under same synthetic condition as 7N-$Cu_3Mo_2O_9$.

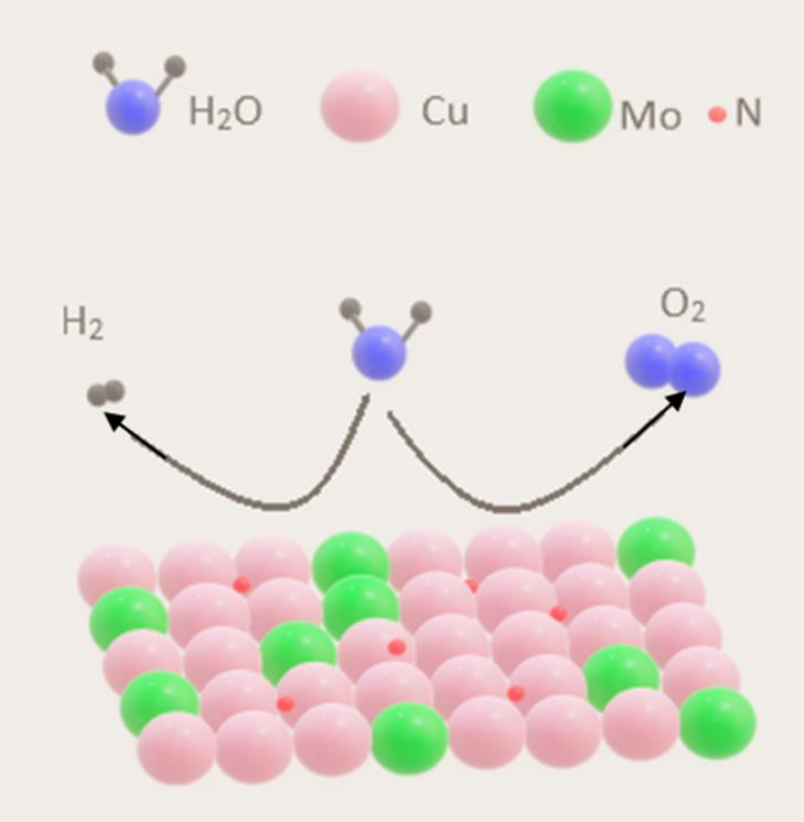


Figure 2.1: Nitrogen dope $Cu_3Mo_2O_9$

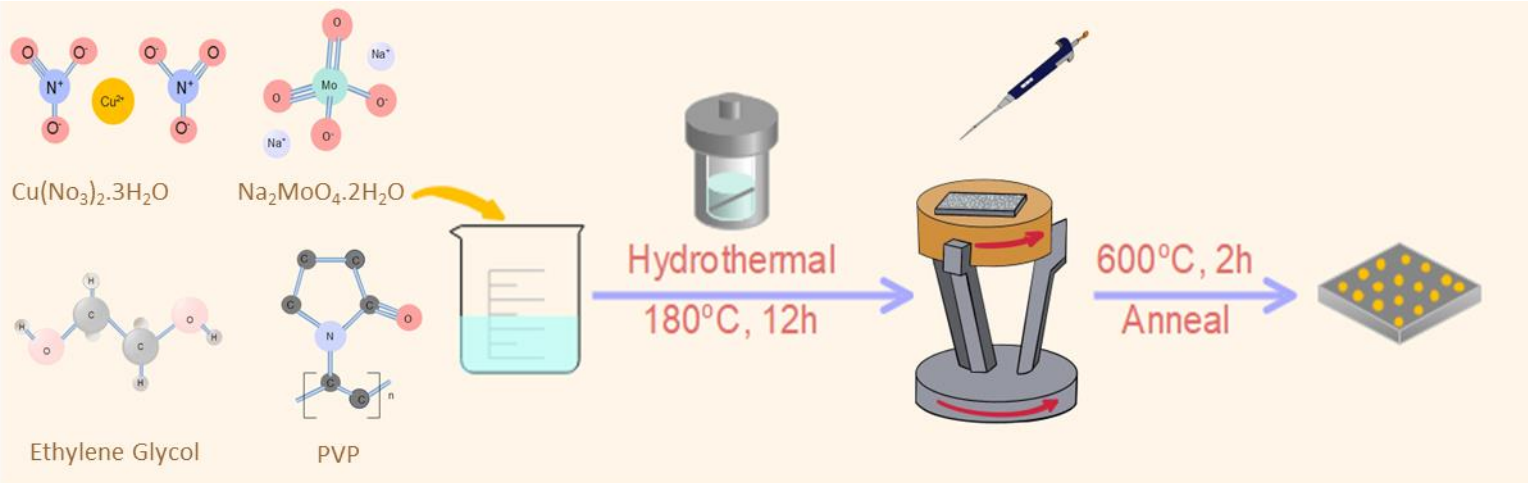


Figure 2.2: synthesis process

**Measurement method**

- Characterization

The nanostructures were observed with a scanning electron microscope (SEM, JEOL JSM-6500F), transmission electron microscope (TEM) and highresolution TEM (HR-TEM) taken on a JEOL, JEM-2100F transmission electron microscope. The X-ray diffraction (XRD) patterns of undoped and doped $Cu_3Mo_2O_9$ samples were measured in range from 10-100o by X-ray diffractometer (D/MAZX 25000V/PC). X-ray photoelectron spectroscopy (XPS; ThermoFisher) measurements were performed using monochromatic AlKα radiation (hν = 1486.6 eV).

- Electrochemical characterizations

All electrochemical performances were characterized by using a standard three-electrode system on electrochemical workstation (Biologic VSP) at room temperature. Typically, the three-electrode cell includes self-support 7N-$Cu_3Mo_2O_9$ on Ni foam as working electrode (area=1x1 cm), a pure graphite rod counter electrode, andan saturated calomel reference electrode (SCE). The all samples were electrochemically tested with the loading mass of 1 mg/cm$^2$. For comparison, Commercial material IrO2 and Pt/C (20 wt%) were used. 5mg material and 25µlnafion 5% were dissolved in 980µlethanol then dropped on NF. All electrochemical measurements were carried out in Ar-saturated 1M KOH as the electrolyte. For HER and OER, the electrocatalytic activity was determined by employing the linear sweep voltametry (LSV) at a scan rate of 5 mVs-1. All recorded potential was converted to reversible hydrogen electrode (RHE) by using Nernst equation as E (vs. RHE) =E (vs. SCE) +0.0591 x pH +0.241 V. The electrochemically active specific area (ECSA) of catalyst sample was determined through the double-layer capacitance (Cdl) which was evaluated by measuring the cyclic volmamogram (CV) at non-faradaic potential with various scanning rates. The ECSA were calculated as follow:

ECSA= Cdl/Cs

Where Cs is defined as capacitance measured on a flat standard of 1cm$^2$ real surface area. In general, Cs is usually 0.0209 mF/cm$^2$ for carbon material.

## 2.3 Results and discussion

### 2.3.1 Physicochemical characterization

According to figure 2.2, the synthetic process of 7N-$Cu_3Mo_2O_9$ is described. Firstly, the bimetallic hydroxide was deposited directly on NF surface under hydrothermal treatment. After covering NF with hydroxide, urea as nitrogen doping agent dissolved in ethanol is coated on NF. Calcination is carried out in order to transform hydroxide to oxide as well as doping nitrogen chemical within bimetallic oxide structure.

The scanning electron microcopy (SEM) and transmittance electron microscopy (TEM) was employed to study morphology of 7N-$Cu_3Mo_2O_9$ under different conditions. As shown as figure 2.3a and 2.3b, SEM images of the sample A-$Cu_3Mo_2O_9$ contains particles on NFandPVP- $Cu_3Mo_2O_9$is stackable nanosheetswhile the Gly-$Cu_3Mo_2O_9$(figure 2.3c) shows arranged nanosheets $Cu_3Mo_2O_9$ to form porous structure on NF. The thickness of nanosheet in PVP- $Cu_3Mo_2O_9$, Glycol $Cu_3Mo_2O_9$ sample are about 3,33nm and 6,3nm respectively while this value in $Cu_3Mo_2O_9$ is 5,7 nm. It can be concluded that PVP affect strongly on the shape of nano sheets. Moreover, the thickness of 7N-$Cu_3Mo_2O_9$ is 2,7nm which is noticeable different form the others. Glycol affects the arrangement of nanosheet of $Cu_3Mo_2O_9$ on NF whereas PVP and Urea control the thickness of nanosheets.Doping Nitrogen stage changes the porous size of the composite which is explain clearly due to BET result. TEM result of 7N- $Cu_3Mo_2O_9$ (figure 2.5a) indicates lattice spacing distance of 3.6Å corresponding to (104) plane of 7N- $Cu_3Mo_2O_9$. From BET result, 7N-$Cu_3Mo_2O_9$ have large surface area. There is noticeable difference between $Cu_3Mo_2O_9$ and 7N-$Cu_3Mo_2O_9$ which is indicated in isothermal graph. Sample 7N-$Cu_3Mo_2O_9$ have surface area is 176.815 $m^2/g$ while this value of $Cu_3Mo_2O_9$ is157.785 $m^2/g$ (fig2.4a) of 2 samples and pore size distribution data. Pore size in $Cu_3Mo_2O_9$ sample distributes from 2 nm to 14 nm, and the mostly pore size is about 10nm to 14nm (figure 2.4b). Pore size of 7N-$Cu_3Mo_2O_9$sample is about under 5nm in the range from 1nm to 35nm (figure 2.4c). EDS mapping directly confirm the component of the composite which include Copper, Molybdenum, Oxygen and

Nitrogen with atomic percentage 21.41%, 15.95%, 57.41% and 5.23% respectively (figure 2.5b-g). This is the important evidence to prove that Nitrogen exists in composite.

To determine crystalline structure of as-obtained bimetallic oxide, XRD measurement was performed to evaluate structure of material. As shown in Figure 2.6, $Cu_3Mo_2O_9$ and 7N-$Cu_3Mo_2O_9$ exhibits clear and sharp peaks, indicating the high quality of crystalline. XRD result is matched with JCPDS No. 00-024-0055. $Cu_3Mo_2O_9$ has specific peak at 12.1, 21.6, 23.1, 25.2, 25.9, 27.0, 29.1 and 35.0corresponding to (020), (130), (200), (131), (002), (104), (112) and (202) planes $Cu_3Mo_2O_9$ which presents Pna21. N-$Cu_3Mo_2O_9$ has dominant facet of (104). In the sample. Gly- Cu3Mo2O9 poses XRD result with mostly facet of (201) and it is different from Cu3Mo2O9 (fig2.6a). the dominant facet of sample 3N,5N and 7N-$Cu_3Mo_2O_9$ is (104) and the amount of Nitrogen does not affect dominant facet

Raman spectrum studying about vibration of $Cu_3Mo_2O_9$ is illustrated in figure 2.7d. In this measurement, laser 520nm is used. According to the spectrum, there are peaks at 335$cm^{-1}$ and 509 $cm^{-1}$ which are represent the vibration mode Eg of $Cu_3O_4$. This can predicts the present of both Cu(I) and Cu(II) in composite. Peak at 811 $cm^{-1}$ and 879 $cm^{-1}$ correspond to stretching mode of Mo-O-Mo bond while 938 $cm^{-1}$ peak is supposed to symmetric stretching mode Mo-O bonds. After doping Nitrogen, the peaks slightly shift to negative direction[34–36] because doping affect causes changes the amount of oxygen of the material

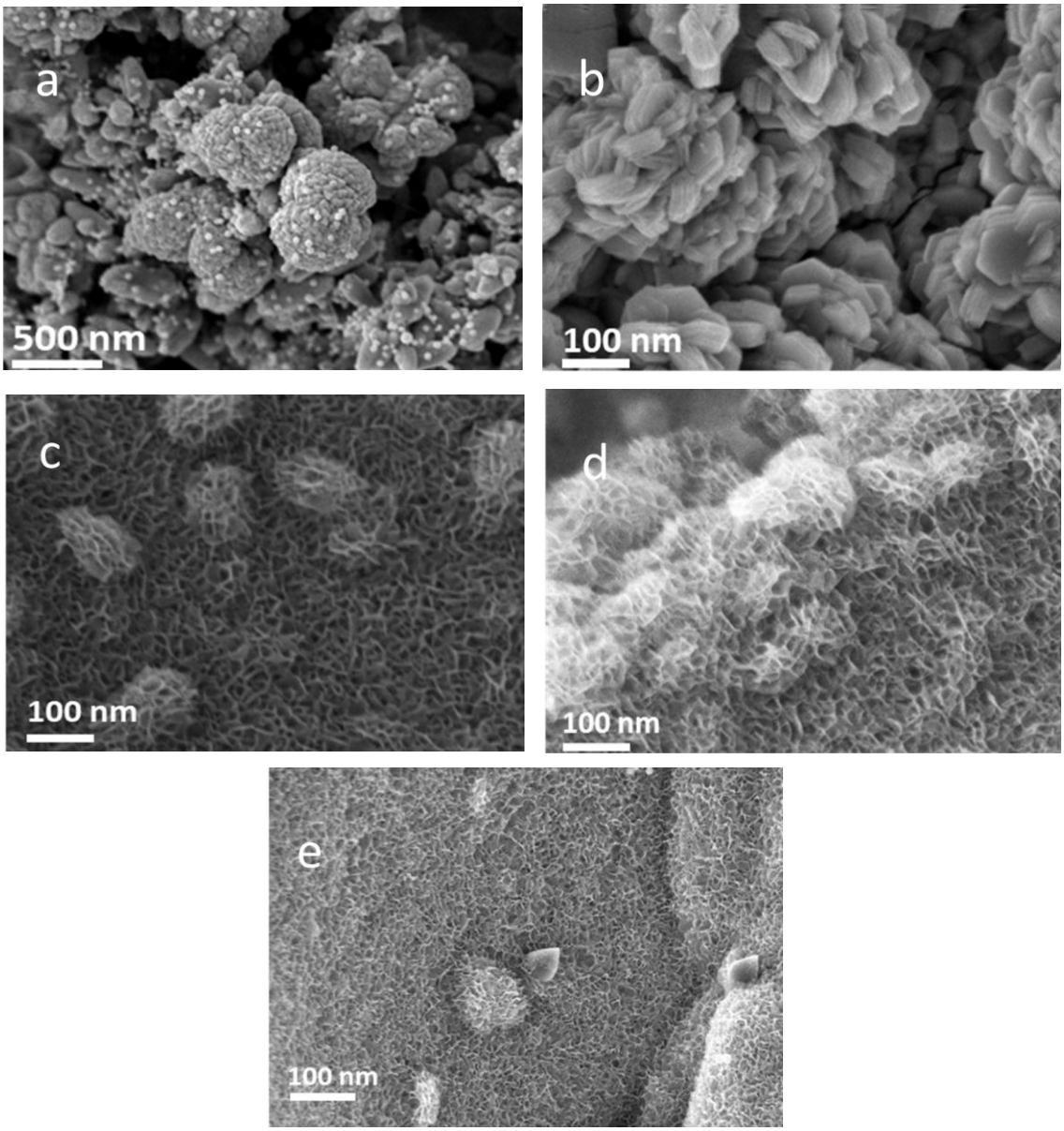


Figure 2.3: SEM images of (a) A- $Cu_3Mo_2O_9$, (b) PVP- -$Cu_3Mo_2O_9$, (c) Gly -$Cu_3Mo_2O_9$, (d) $Cu_3Mo_2O_9$, (e) 7N- $Cu_3Mo_2O_9$

The chemical state of surface can be studied according to XPS (Figure 2.7),Mo3d spectra (figure 2.7 b) shows 2 peak which represent for the existence of Mo(IV) and Mo(VI) in samples $Cu_3Mo_2O_9$.the result indicates the different intensity of Mo(IV) and Mo(VI) when doping nitrogen  However, Mo3d spectra of 7N-$Cu_3Mo_2O_9$ does not exhibit specific peak at 229eV[37,38]which point out the present of Molybdenum and Nitrogen bond. It can be predicted that Nitrogen did not create chemical bond with Molybdenum. Next, Copper 2p spectra (figure 2.7a) describes copper state in $Cu_3Mo_2O_9$ with peak at 932,933 eV corresponding to Cu(I),Cu(II) (Cu $2p_{3/2}$) while peak at 953 eV belongs to Cu $2p_{1/2}$ (including Cu(I) and Cu(II)). Peaks at 942 eV and 961.8eV express Cu(II) satellite.Besides, Copper-Nitrogen bond also expect to present in copper spectra. As describe, in figures, 7N-$Cu_3Mo_2O_9$ show peak at 934.8eVwhich is specific peak for Copper and Nitrogen bond[39,40]. Additionally, Nitrogen 1s spectra (figure 2.7c)has peak at 397.83 eV which is present for Metal-Nitrogen bond, in this situation Copper and Nitrogen bond is discussed. XPS data proves that Nitrogen successfully doped in composite by this method and Nitrogen-copper formation

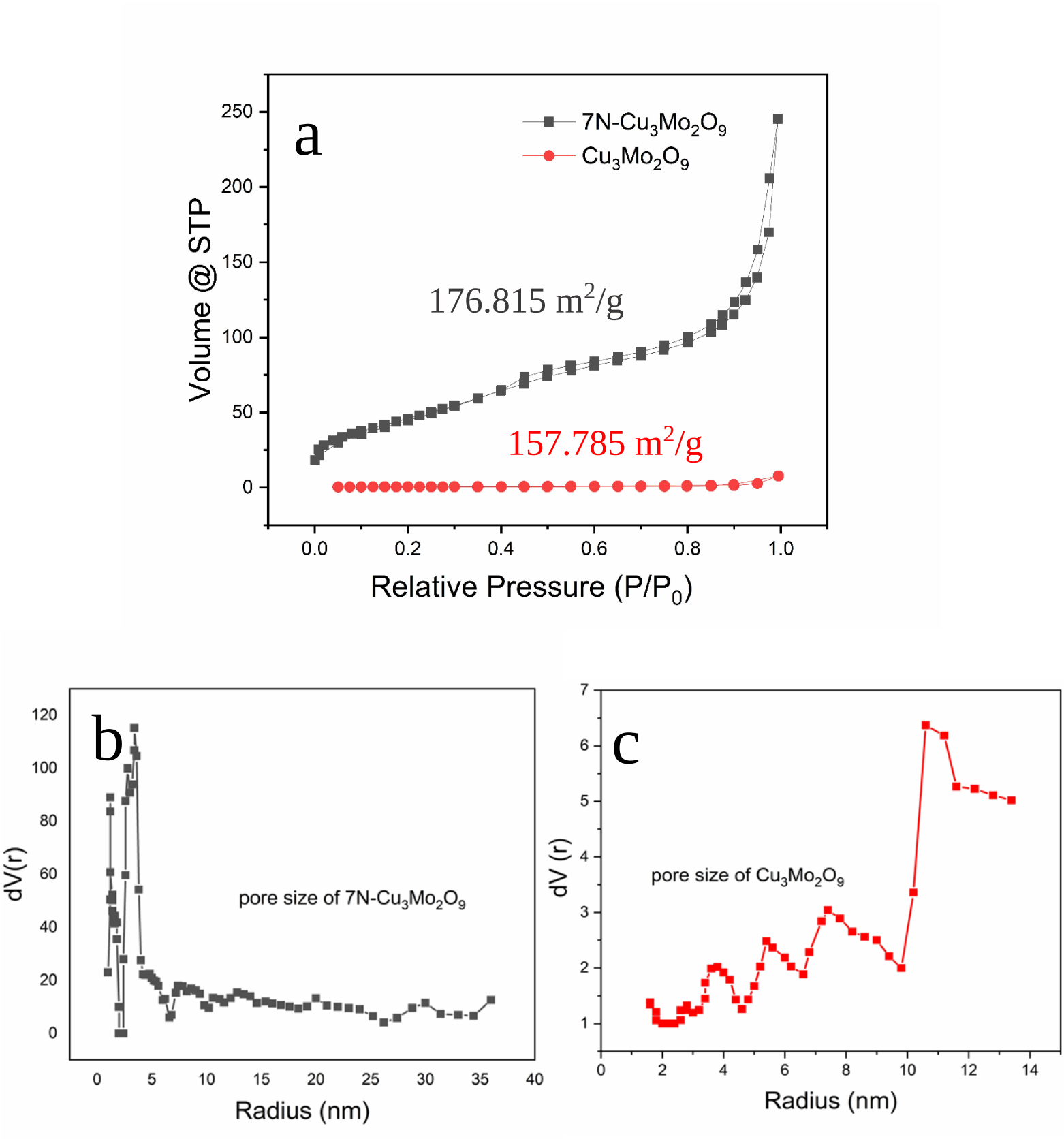


Figure 2.4: BET result (a) isotherm (b) pore size of Cu3Mo2O9,(c) pore size of 7N-Cu3Mo2O9

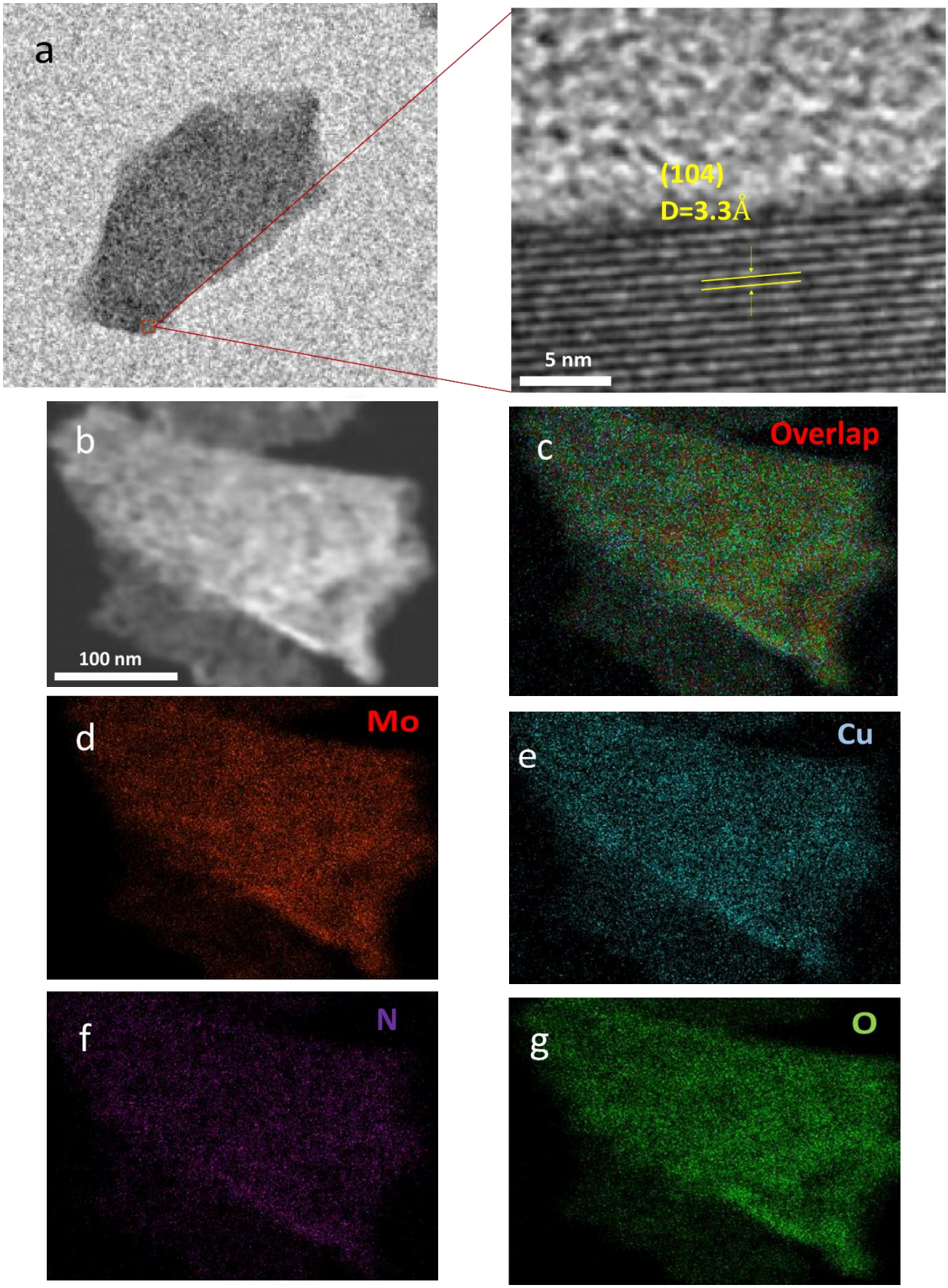


Figure 2.5: (a) TEM images of 7N-Cu3Mo2O9, (b)-(g) Elemental mapping

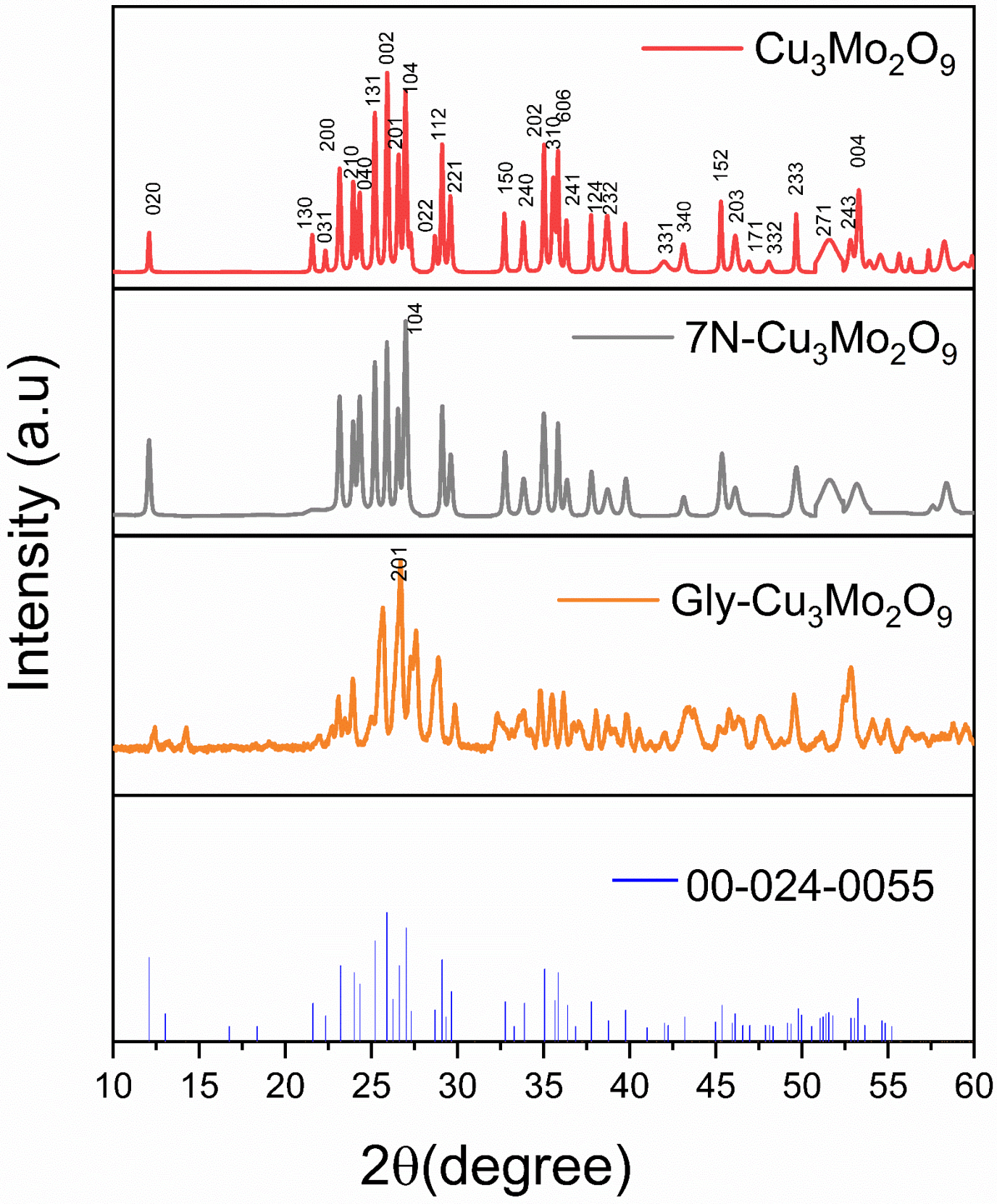


Figure 2.6: XRD spectra (a)

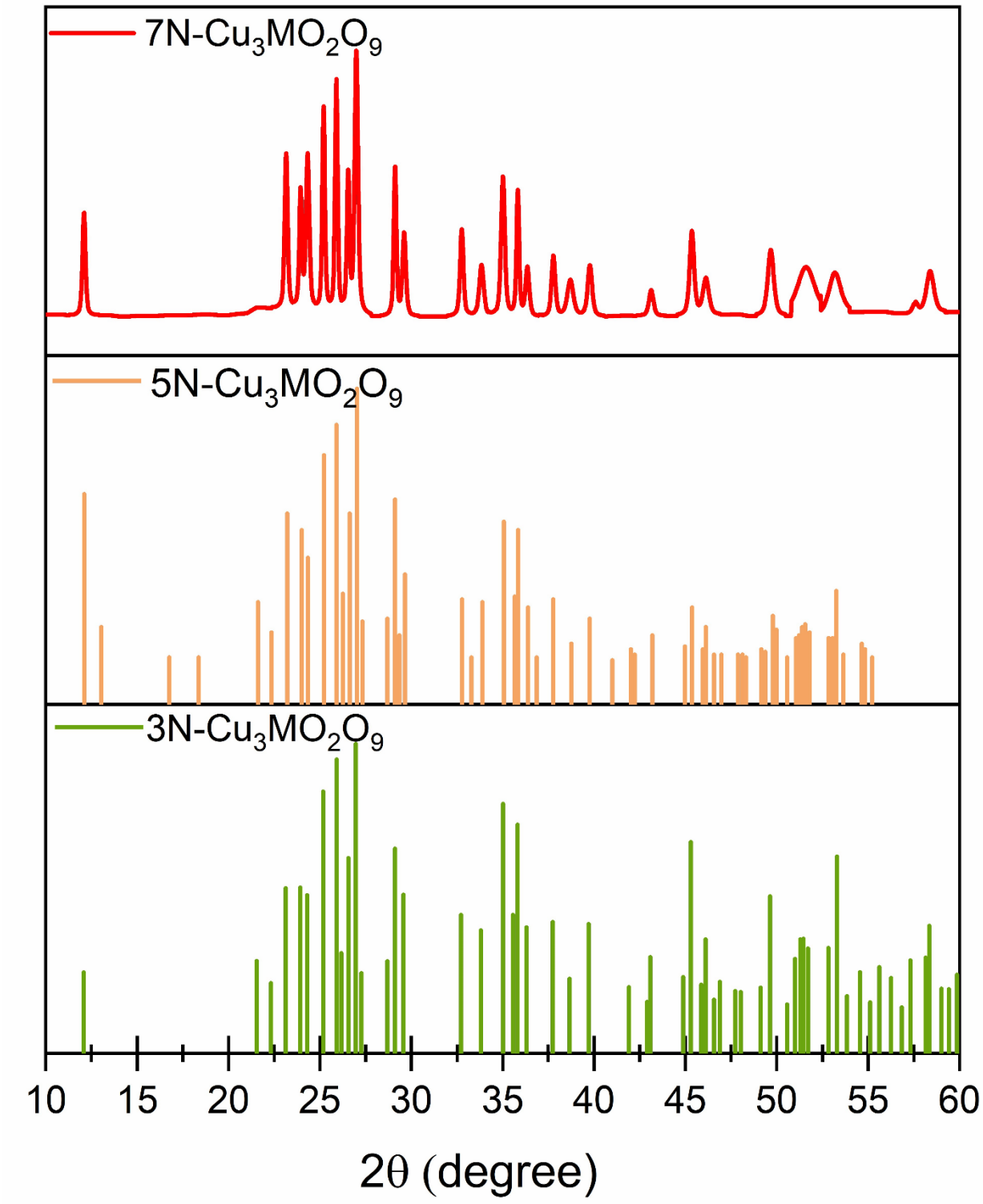


Figure 2.6: XRD spectra (b) Nitrogen dope

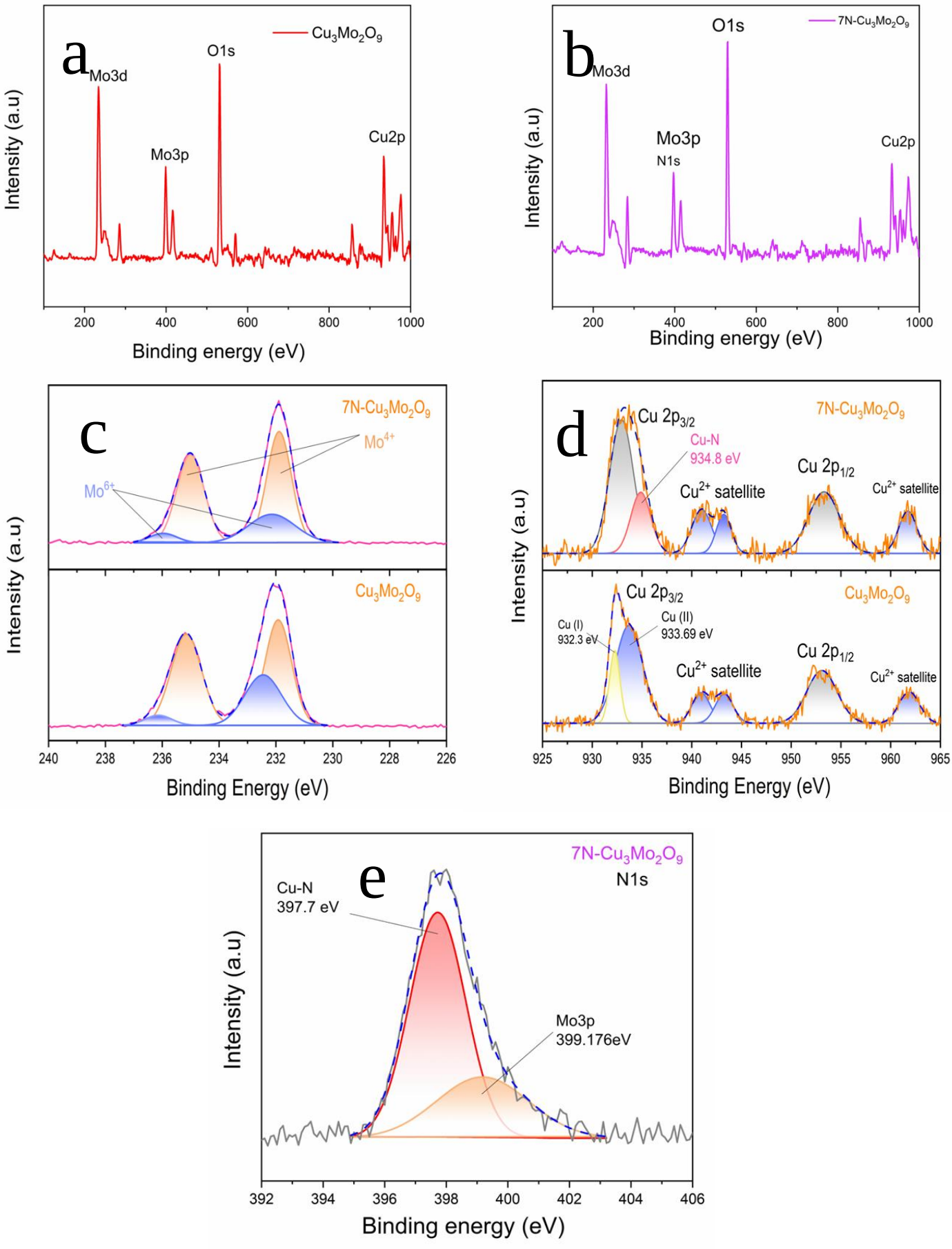


Figure 2.7: XPS spectra, widerange (a)$Cu_3Mo_2O_9$,(b)7N-$Cu_3Mo_2O_9$;(c) Molybdenum, (d)Copper; (e) Nitrogen

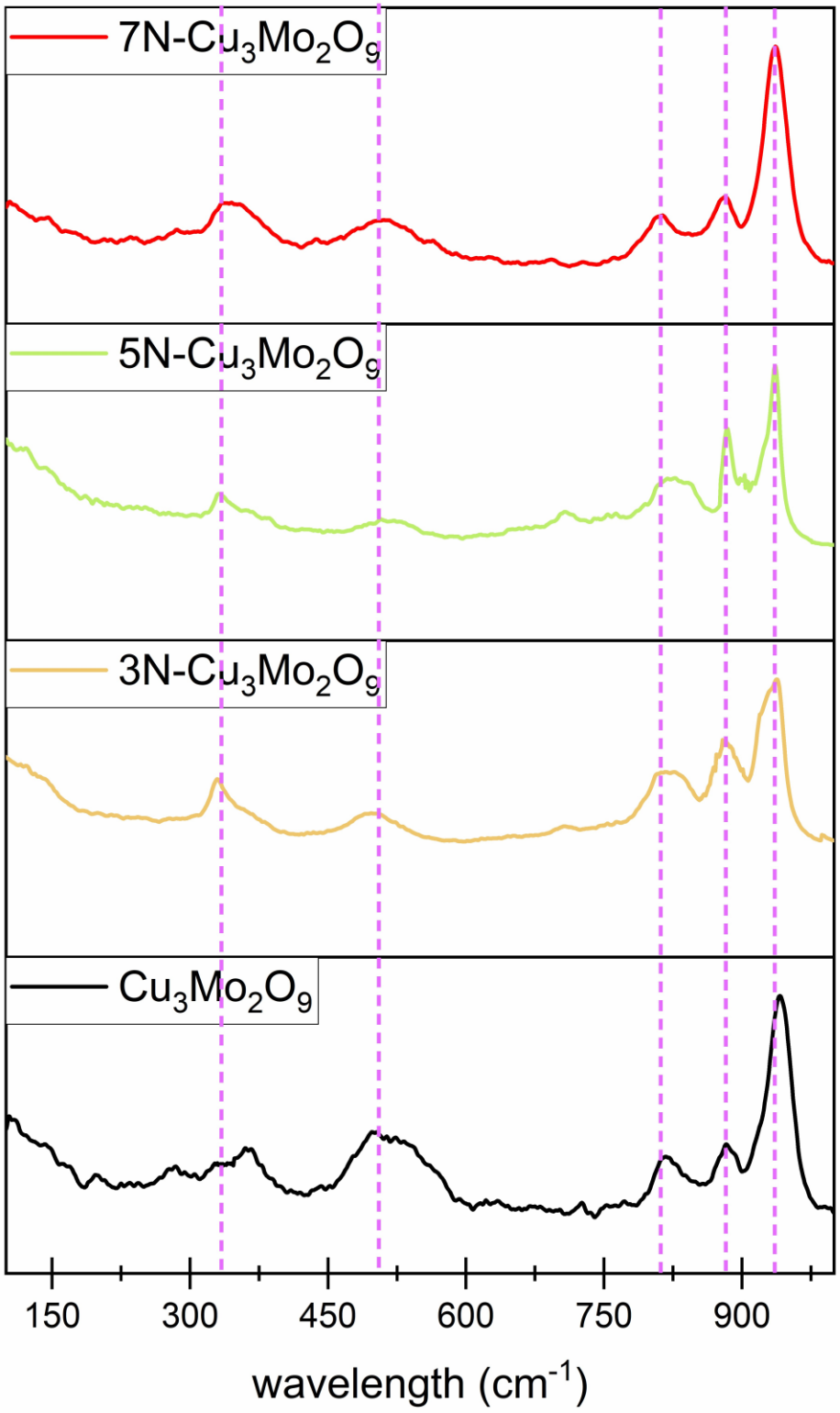


Figure 2.8: raman

2.3.2 Electrochemical performance

According to following data, it is revealed that glycol and PVP affect morphology of the material from that lead to the enhancement of catalyst activity. Glycol role is to control the material arrangement. Bimetallic source will dispose to porous shape on NF surface that leads to the higher surface area formation which is one of morphology properties effect water splitting catalyst material.

PVP affects the formation of $Cu_3Mo_2O_9$ crystal. PVP and Ethylene glycol control the facet of $Cu_3Mo_2O_9$ crystal which is supposed to influence water splitting. After determining the, the role of PVP and ethylene glycol, the ratio of Nitrogen dope $Cu_3Mo_2O_9$ are optimized by various Urea amount to evaluate and comparison with commercial material

For HER test, LSV curves of various doping content sample were displayed in figure 2.8a. In particular, 7N-$Cu_3Mo_2O_9$ shows the best onset potential (12mV) while the second candidate is commercial material Pt/C (30mV). However, in higher current, Pt/C cannot perform as well as 5N-$Cu_3Mo_2O_9$. This is proved by overpotential at 15mA: 7N-$Cu_3Mo_2O_9$ (57V), 5N-$Cu_3Mo_2O_9$ (149mV) and Pt/C (155mV) Moreover, to evaluate kinetic of the reaction, Tafel slope is necessary parameter (figure 2.8b). The lower Tafel slope value is, the faster reaction happens. 7N- $Cu_3Mo_2O_9$sample had the most ideal Tafel slope value for HER with 65mVdec$^{-1}$ while 5N- $Cu_3Mo_2O_9$, 3N- $Cu_3Mo_2O_9$, $Cu_3Mo_2O_9$ and Pt/C are139 mVdec$^{-1}$,165 mVdec$^{-1}$, 203 mVdec$^{-1}$ and 71 mVdec$^{-1}$ respectively.

As the result, HER with 7N- $Cu_3Mo_2O_9$catalyst is the fastest in this evaluation. ECSA (Figure 2.8d) is also study in this research. From ECSA data, the double layer capacitance ($C_{dl}$) is calculated. ECSA is linear graph and the slope value of that line is $C_{dl}$. 7N- $Cu_3Mo_2O_9$is still the best option for electrocatalyst base on the highest $C_{dl}$ value (1.42 mFcm$^{-2}$). Next, EIS data are mentioned (figure 2.8c). EIS data support information about charge transfer resistance ($R_{ct}$) and Rs of the material which relate to kinetic of the reaction. 7N- $Cu_3Mo_2O_9$ sample exhibit $R_{ct}$=0.8169Ω which are the lowest value in the series. Mass activity of material graph illustrates that 7N-$Cu_3Mo_2O_9$ sample has outstanding HER performance according to mass. Besides, oxophilic metal Molybdenum support catalyst in balancing OH* and H* in order to improve active size issues in catalyst. SEM indicates the

thin thickness of nanosheets when Urea joins process. Thin nanosheets can provide larger active area and it is also convenient for charge transfer kinetic due to short distance. [43]

Additionally, stability test is one of the essential to criterion when there is a competition between new generation material and commercial material. Herein, CP test is used for sample 7N- $Cu_3Mo_2O_9$ and Pt/C (20wt%) in the same condition (KOH 1M, 80 hours, room temperature) (figure 2.10a). The current of 100mA is applied for the system and the potential in the system will be recorded according to time. 7N- $Cu_3Mo_2O_9$ exhibit excellent stability which almost did not change after 80 hours (from -0.38V to -0.35V) while this value of Pt/C decrease 37% (drop from -0.45V to -0.72V)

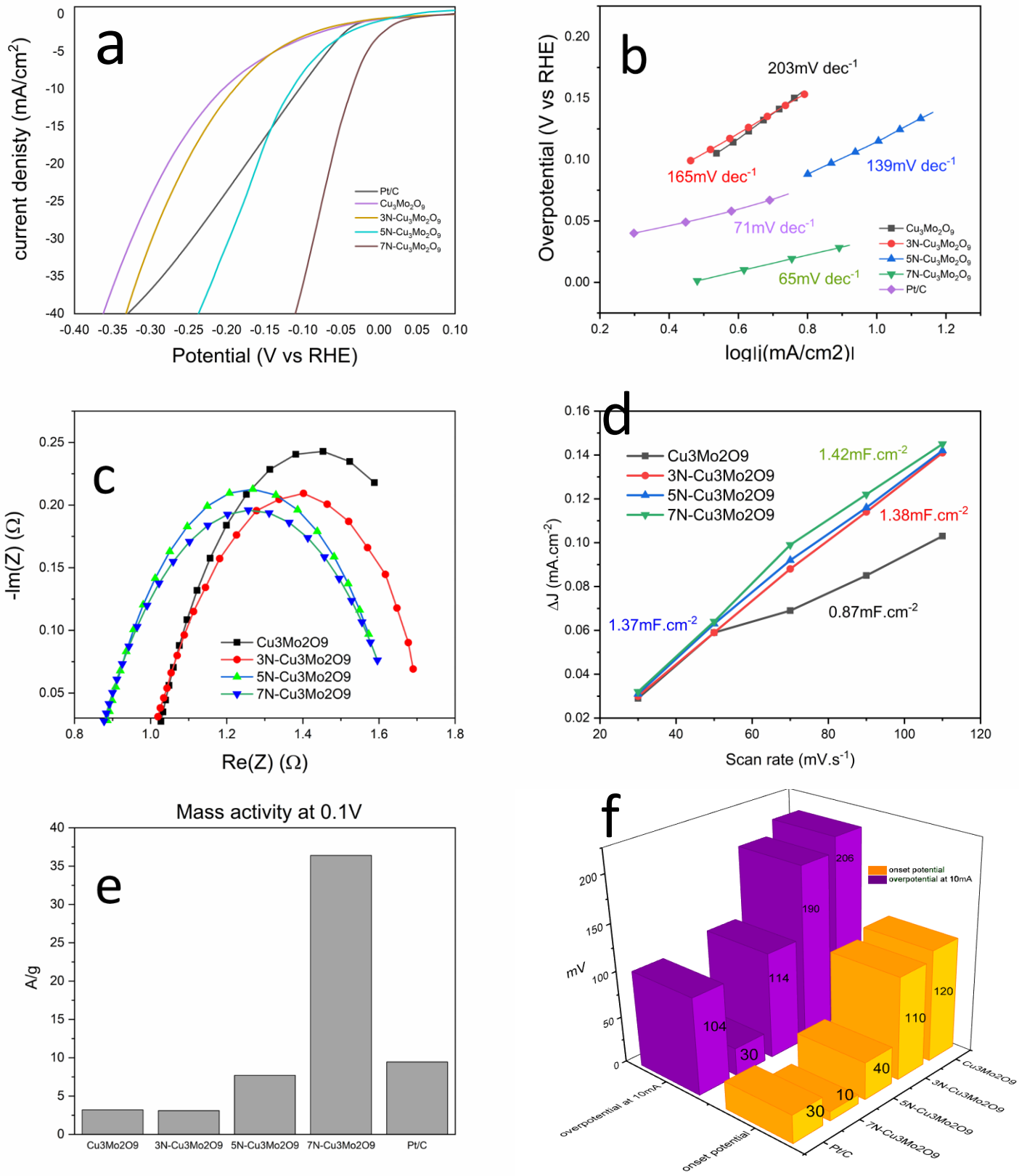


Figure 2.9: HER performance (a) LSV, (b) Tafel slope, (c) EIS, (d) ECSA, (e) Mass activity, (f) overpotential

| sample | Overpotential at 10mA (mV) | Tafel slope | reference |
|---|---|---|---|
| MoP/$Ni_2$P/NF | 75 | 100 | 42 |
| Cu-CMP850 | 350 | 135 | 43 |
| Ni/$Mo_2C$ | 179 | 101 | 44 |
| NiMoN-550 | 89 | 79 | 45 |
| MoPNA/CC | 80 | 83 | 46 |
| 7N-$Cu_3Mo_2O_9$ | 30 | 65 | This work |

Table 2.1: HER efficiency comparison

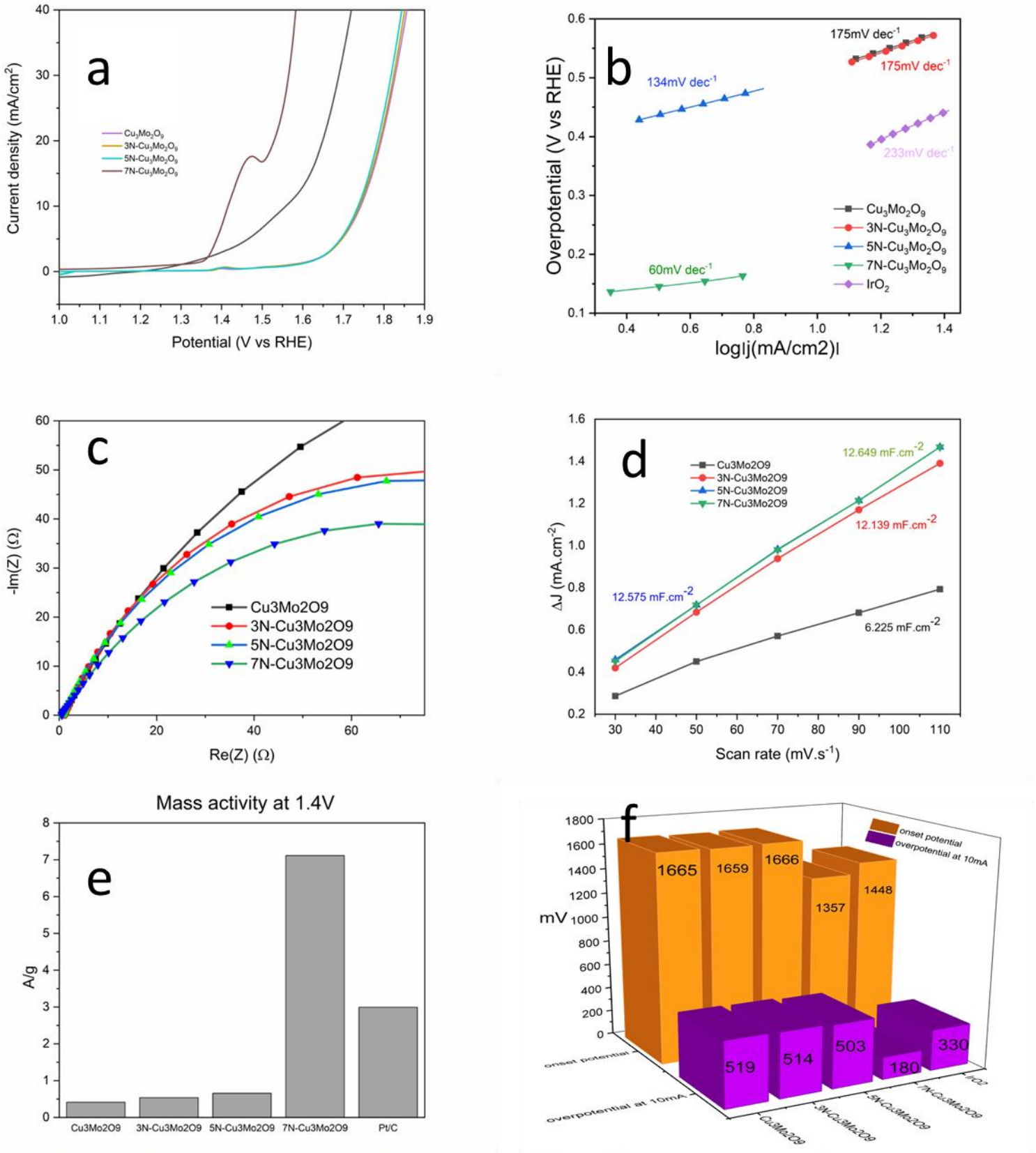


Figure 2.9: OER performance (a) LSV, (b) Tafel slope, (c) EIS, (d) ECSA, (e) Mass activity, (f) overpotential

| sample | Overpotential at 10mA (mV) | Tafel slope | reference |
|---|---|---|---|
| Cu-CMP850 | 450 | 62 | 44 |
| Cuo-Cu bird | 580 | 90 | 49 |
| $CoMoS_4$/CC | 342 | - | 50 |
| $CoMoS_4$/Ni3S2 | 200 | - | 51 |
| $CoMoS_4$/NF | 250 | - | 52 |
| 7N-$Cu_3Mo_2O_9$ | 180 | 60 | This work |

Table 2.2: OER efficiency comparison

For OER, 7N- $Cu_3Mo_2O_9$ sample continuously performs its strong electrocatalyst function with overpotential (figure 2.9a); at 10mA (180mV) and this value is more outstanding than the others as $IrO_2$ (330mV),5N- $Cu_3Mo_2O_9$(503mV), 3N- $Cu_3Mo_2O_9$ (514mV) and $Cu_3Mo_2O_9$ (519mV). The mass activity also indicates efficiency of composite base on amount of material. As can be seen, the graph (figure 2.9e) shows that 7N- $Cu_3Mo_2O_9$ is the best material for OER with 7.11A/g while commercial material is just about 2.99A/g this value of samples decreases when the ratio of Nitrogen amount in the sample decreases from 7N- $Cu_3Mo_2O_9$ to $Cu_3Mo_2O_9$. Tafel slope and EIS are 2 performance which is used to evaluate kinetic of OER. Tafel slope of 7N- $Cu_3Mo_2O_9$ express the lowest value 60mVdec$^{-1}$(figure 2.9b). The following competitors are IrO2 (233mVdec$^{-1}$), 5N- $Cu_3Mo_2O_9$(134mVdec$^{-1}$), 3N- $Cu_3Mo_2O_9$ (175mVdec$^{-1}$) and $Cu_3Mo_2O_9$ (175mVdec$^{-1}$) catalyst. The high resistant is unexpectable data in electrocatalyst detailly in OER. From figure 6c, it shows that 7N- $Cu_3Mo_2O_9$ posed the smallest Rct (139.6Ω) which means electron more easily transfer through the composite the others.

Long-term performance test for OER is carried out by chronopotentiometry for 80h at current density of 100 mA/cm$^2$ (1M KOH) (figure 2.10b). After the test, the delivered potential of 7N- $Cu_3Mo_2O_9$ is nearly the same from 1.96mV to 1.91mV. These data also proves that the benefit of building directly the material on NF surface in the composite synthesis process.

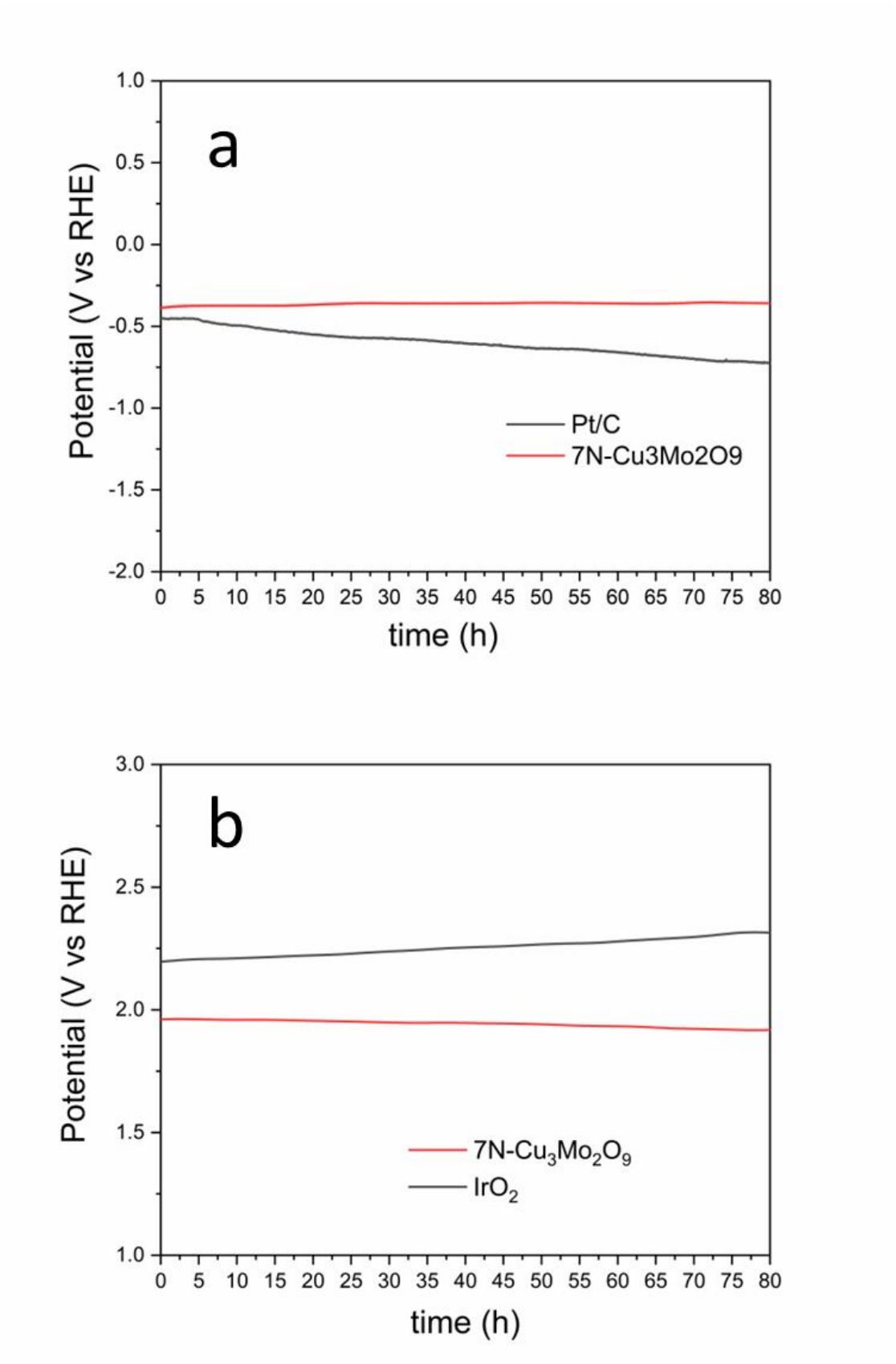


Figure 2.11: Stability test (a) HER, (b) OER

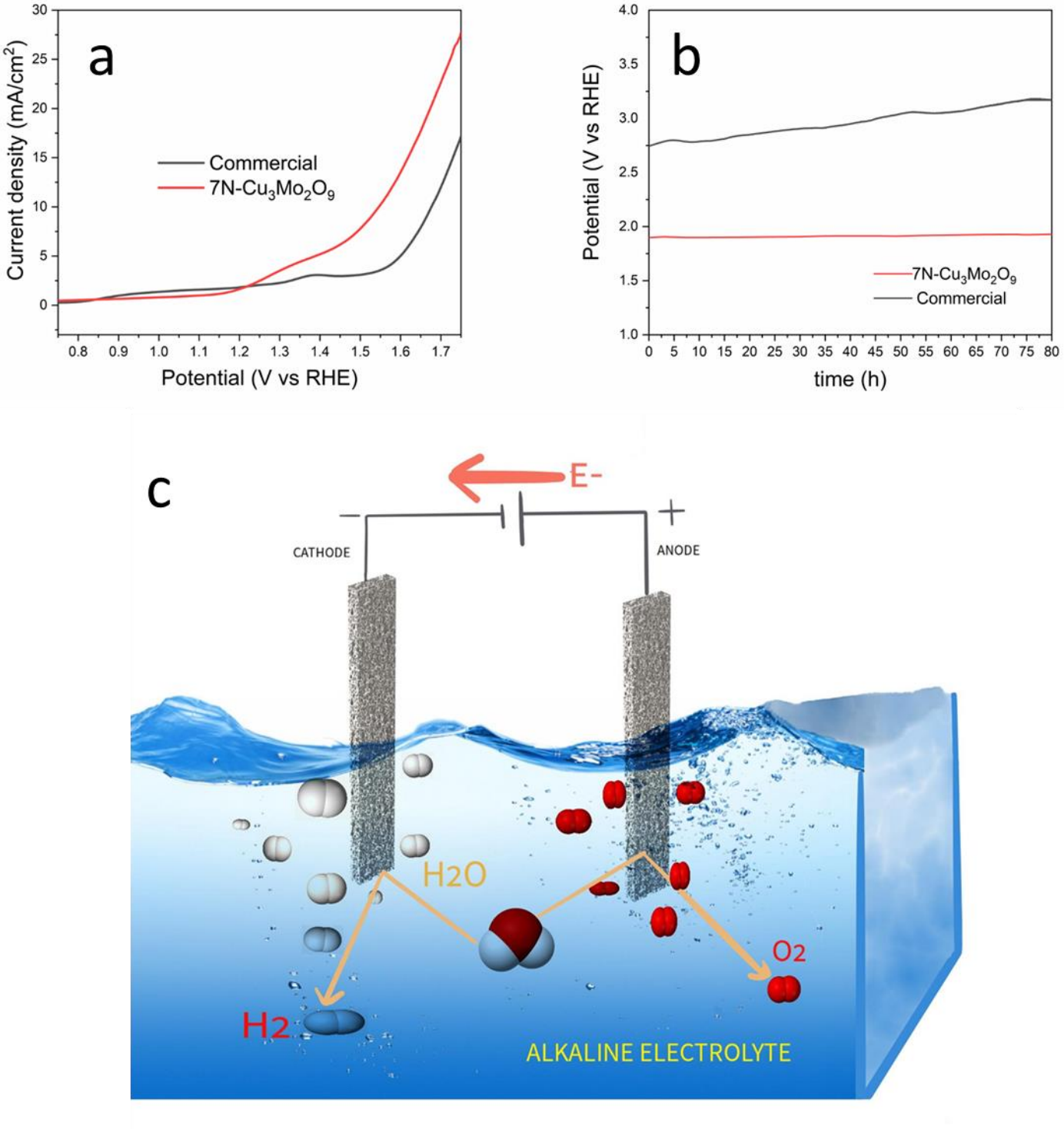


Figure 2.12: Overall water splitting (a) LSV, (b) Stability, (c) OWS illustration

| sample | Overpotential at 10mA (mV) | reference |
|---|---|---|
| $NiCo_2S_4$NW | 400 | 53 |
| $Ni_3S_2$ | 500 | 53 |
| $NiCo_2O_4$ | 610 | 53 |
| $Ni_3Se_2$/Cu | 420 | 54 |
| NiS | 410 | 55 |
| 7N-$Cu_3Mo_2O_9$ | 155 | This work |

Table 2.3: OWS efficiency comparison

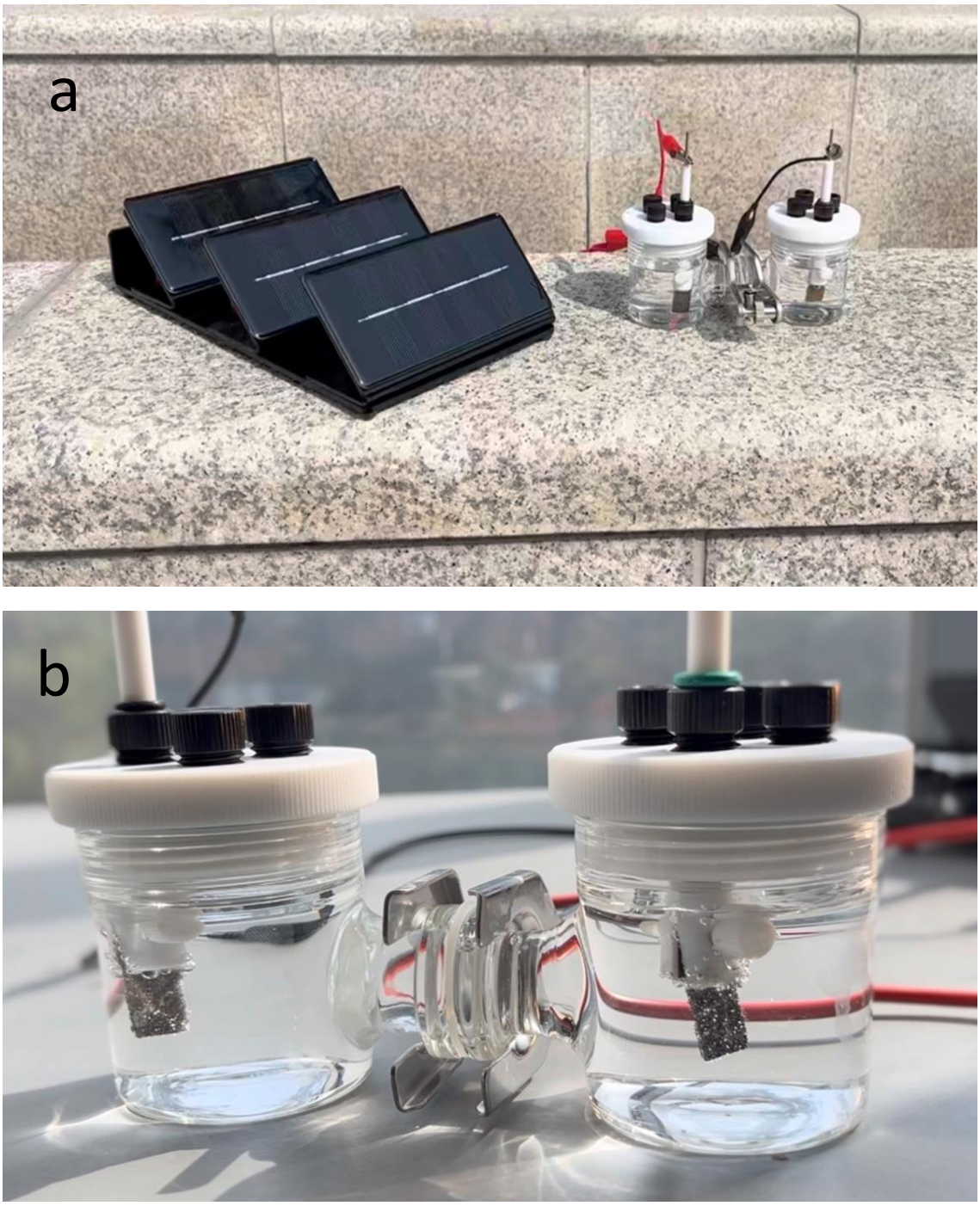


Figure 2.13: (a) OWS working by solar system, (b) 2 electrode in OWS

Based on all good HER and OER activity above system data, overall water splitting (OWS) self-assembly cell is constructed by 7N- $Cu_3Mo_2O_9$ based-on two-electrode system. LSV curve (figure 2.11a) reveals that 7N- $Cu_3Mo_2O_9$-baseelectrolyzeris more efficient than Pt/C ‖ $IrO_2$. The overpotential at 10mA of product is 155mV and this is 167mV for Pt/C ‖ $IrO_2$. Stability (figure 2.11 b) is also study for this part. The activity of 7N- $Cu_3Mo_2O_9$ went down 1.56% from 1.89V to 1.92V in 80 hours

Density function theory (DFT) calculation was performed by using plane-wave Quantum-ESPRESSO packages. The Bayesian error estimation functional with a Van Der Waals-corrected exchange correlation functional (BEEF-vdW) was employed to accurately obtain chemisorptions and absorption energy on the surface. The interaction between the valence and core electrons was computed through ultrasoft pseudopotential approach. The energy cutoff of the wavefunction and charge density were set in range of 50 to 200 Ry, respectively. The convergence criteria for electronic structure iterations and force on each atom during structure relaxation were set to $10^{-9}$ Ry and $10^{-4}$ Ry/Bohr, respectively. For geometry optimization, all structure models are sampled by Brillouin zone with 8x8x1 Monkhorst-Pack k-point mesh to obtain convergence of total energy. 20 $A^o$ vaccum in Z-direction was added to avoid the interaction between periodic images. All computations were performed under spin polarization.

The change in Gibb free energy for each steps of OER was calculated by using computational hydrogen electrode developed by Nørskov. The four-electron OER pathways can be divided into 4 steps:

$$* + OH^- \rightarrow OH^* + e^- \quad (1)$$

$$OH^* + OH^- \rightarrow O^* + H_2O + e^- \quad (2)$$

$$O^* + OH^- \rightarrow OOH^* + e^- \quad (3)$$

$$OOH^* + OH^- \rightarrow * + O_2 + H_2O + e^- \quad (4)$$

Where * is corresponding to active site on the catalyst surface and OH*, O*, and OOH* stands for adsorbed oxygenated intermediates.

The Gibbs free energy of the catalyst was calculated by following equations:

$$\Delta E_{ads} = E_{catalyst\text{-}H^*} - E_{catalyst} - \tfrac{1}{2} E_{H2} \quad (5)$$

$$\Delta E_{H^*} = \Delta Eads + \Delta E_{ZPE} - T\Delta S \quad (6)$$

Where $E_{catalyst\text{-}H^*}$ donates the total energy of modeled catalyst with absorbed H state, $E_{catalyst}$ stands for the energy of catalyst with bare surface, and $E_{H2}$ is the energy of hydrogen in gas phase. The Gibbs free energy was calculated under conditions of zero-point energy (ZPE) and entropy corrections for hydrogen evolution reaction. $\Delta E_{ZPE}$ is the different in zero-point energy. $\Delta S$ is entropy change between absorbed and gaseous hydrogen and T donates the temperature equaled to 298K. $\Delta E_{ZPE}$ is near 0.04 eV and $\Delta S$ is around 0.2 eV. The reaction free energy is computed by following:

$$\Delta E_{H^*} = \Delta Eads + 0.24 \text{ eV} \quad (7)$$

To get insight into the intrinsic electrocatalytic reactivity and origin of highly efficient HER and OER, the DFT computation was performed to study free energies of HER/OER reaction mechanism at different sites of (104) N-$Cu_3Mo_2O_9$ and (002) $Cu_3Mo_2O_9$ models after geometry optimization, as illustrated in Figure. 1. In Figure 2.15 a, compared with Mo and N sites, the Cu site reveals the highest water adsorption energy, The computed HER free energy diagram of all samples is displayed in Fig2 b. On the line with previous study, suitable ΔGH* for good HER should be close to zero value. Too negative ΔGH* can cause strong bonding between H atom and caytalyst surface, thus leading to difficult desorption, while large positive value indicates weak bonding. Compare with other active sites, the N N-$Cu_3Mo_2O_9$ in structure exhibits the most optimal free energy ΔGH* value of -0.17 eV near Zero, demonstrating the superior HER catalytic activity. As shown in Figure 2.16, the HER mechanism may be proposed that the Cu and N site expedite the decomposition step (Heyrovsky step) and hydrogen formation step (Tafel step), respectively. For OER catalytic mechanism, Gibbs free energy diagram were computed at U=0V, as depicted in Figure.3. All structures have uphill free energy diagrams at two first steps (1.OH- to OH*, 2.OH* to O*), suggesting that these pathways are

endothermic process as active energy barrier and determinate rate. In particular, the Mo sites neighbored N shows the lowest active energy barrier than that of Mo site in $Cu_3Mo_2O_9$, demonstrating that Mo in N-$Cu_3Mo_2O_9$ dominate OER reaction at Anode. All these above evidences is consistence with experimental excellent HER and OER activity.

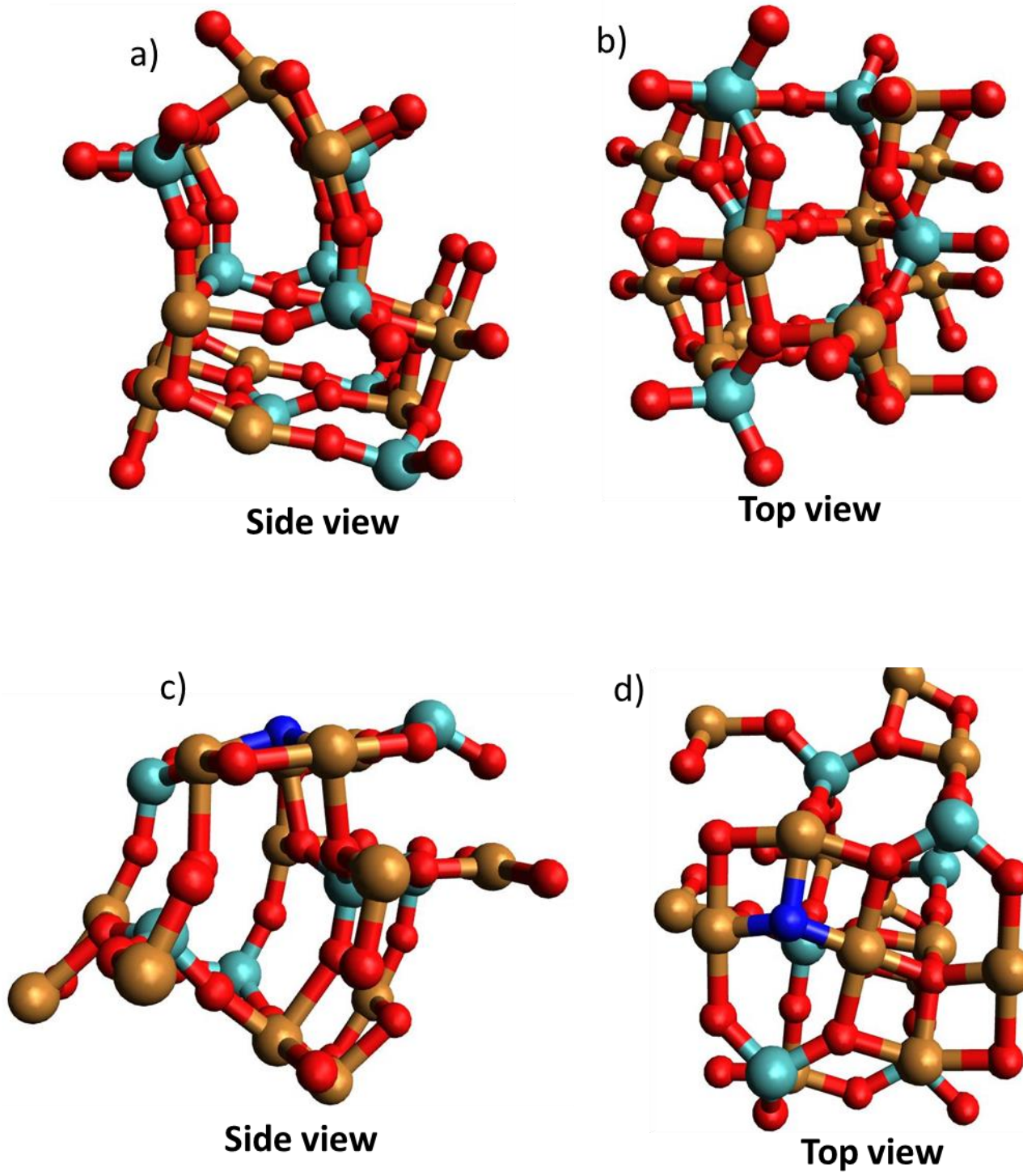


Figure 2.14. Top view (a) and side view (b) of $Cu_3Mo_2O_9$ (002) crystal facet after optimized geometry. Top view (c) and side view (d) of N doped $Cu_3Mo_2O9$ (104) crystal facet after optimized geometry.

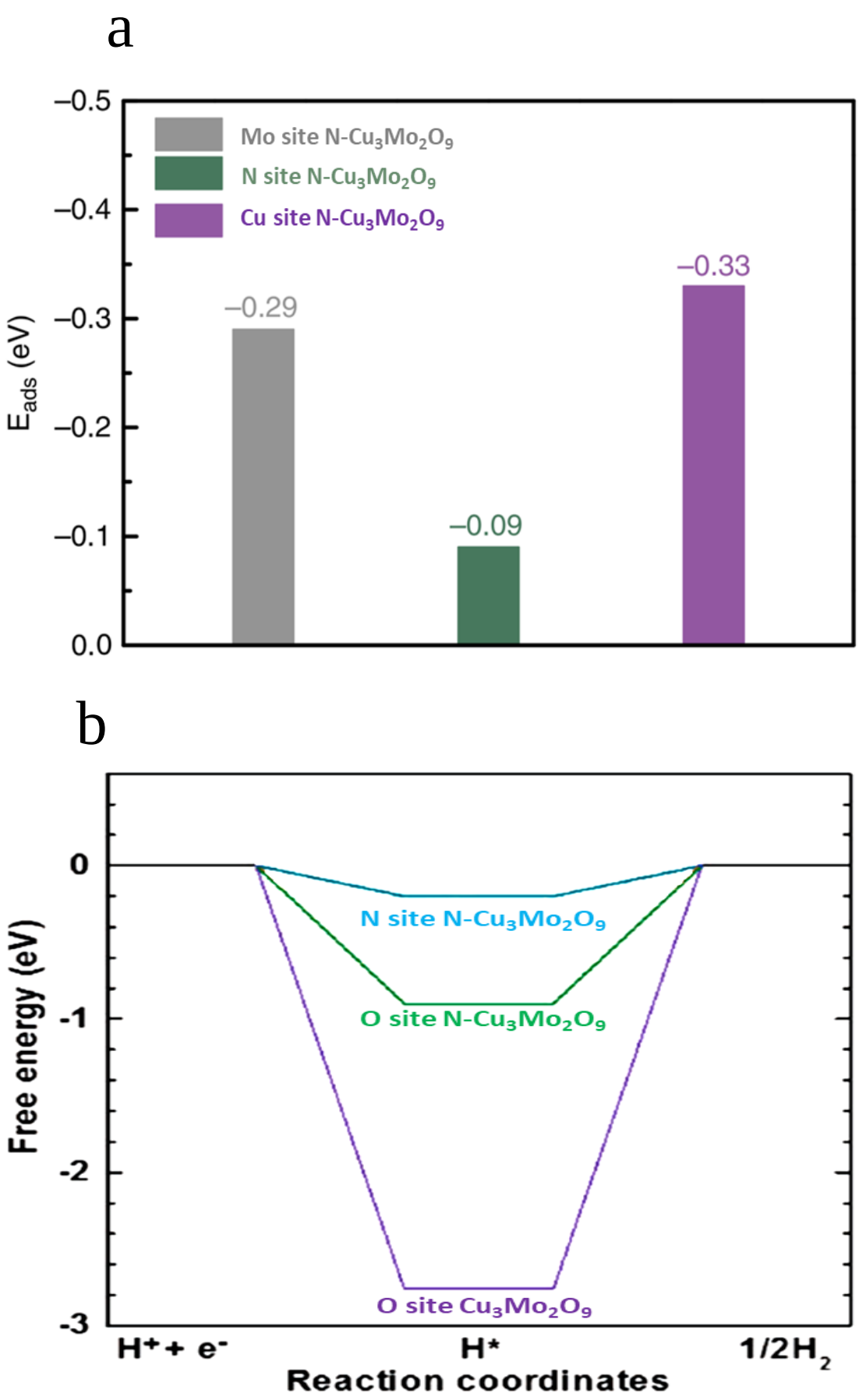


Figure 2.15 (a) Water adsorption energy and (b) hydrogen adsorption/desorption free energy at different sites of N doped $Cu_3Mo_2O_9$ structure.

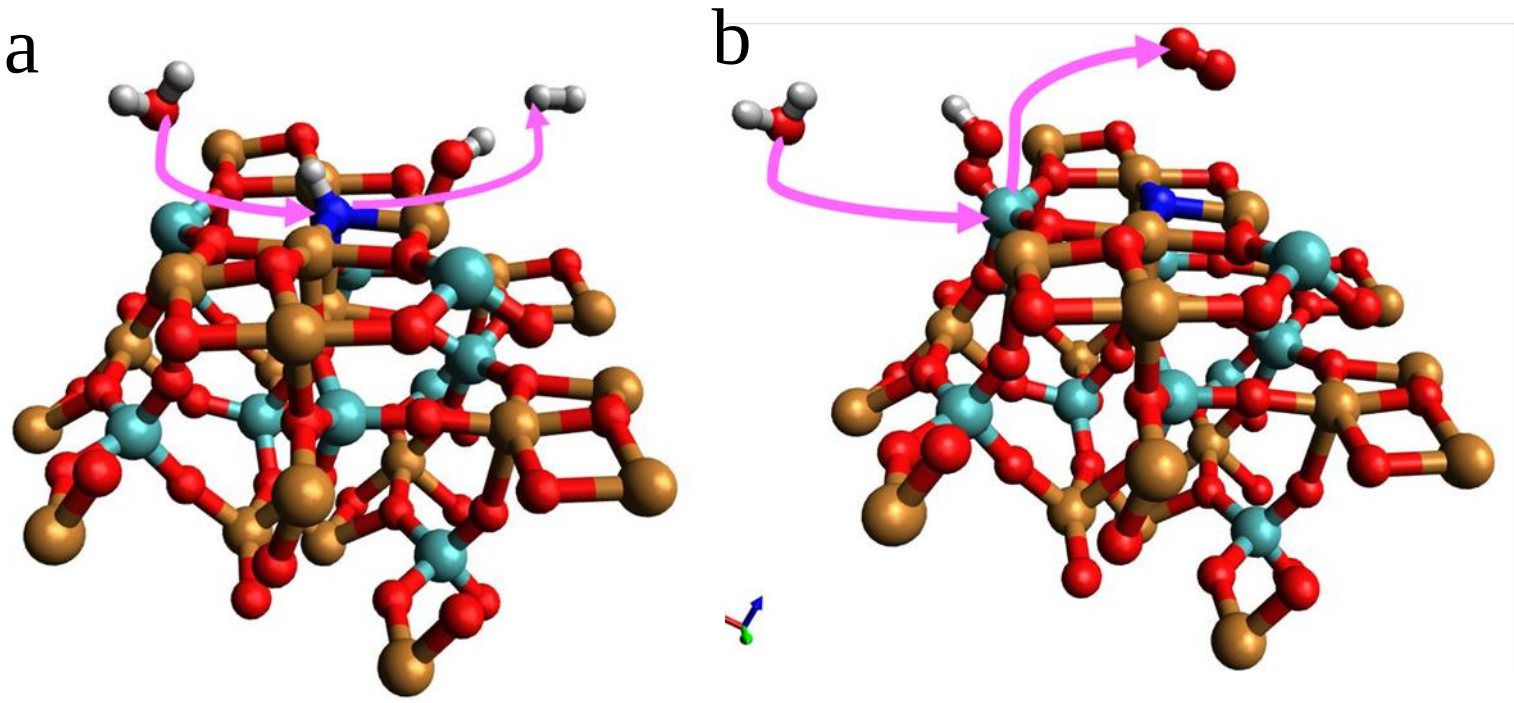


Figure 2.16: Nitrogen dope $Cu_3Mo_2O_9$ mechanism (a)HER (b)OER

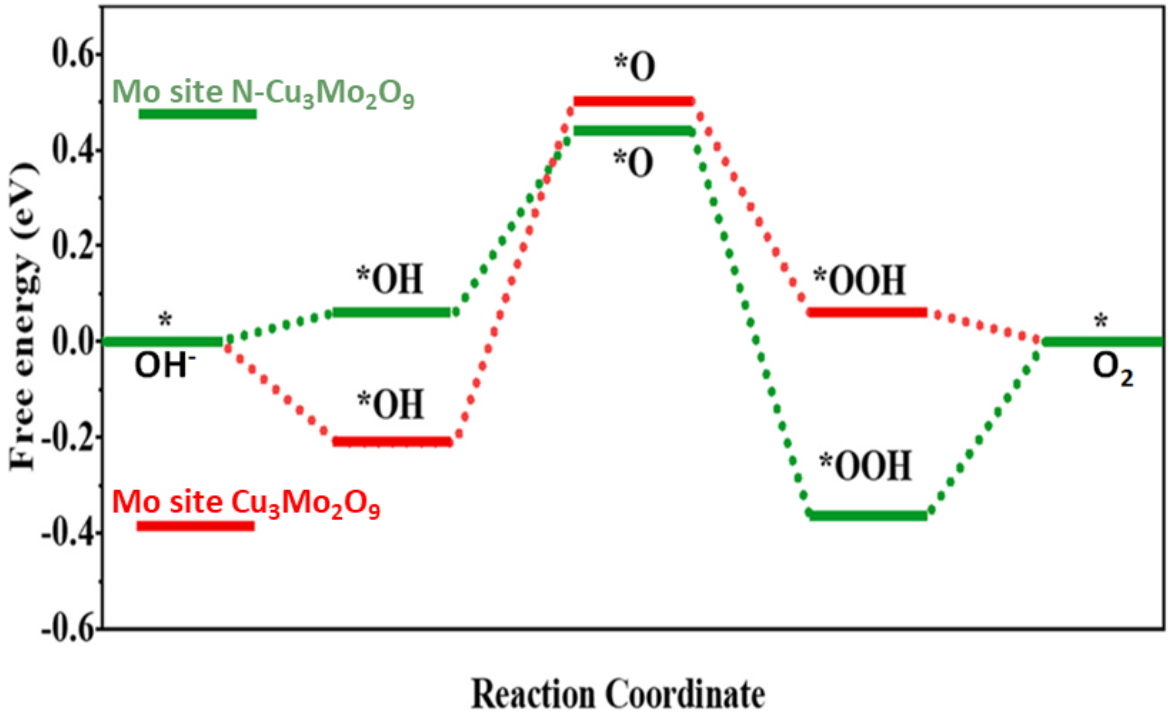


Figure 2.17. Gibb free energy diagram on $Cu_3Mo_2O_9$ structure (red line) and N doped $Cu_3Mo_2O_9$ structure (green line).

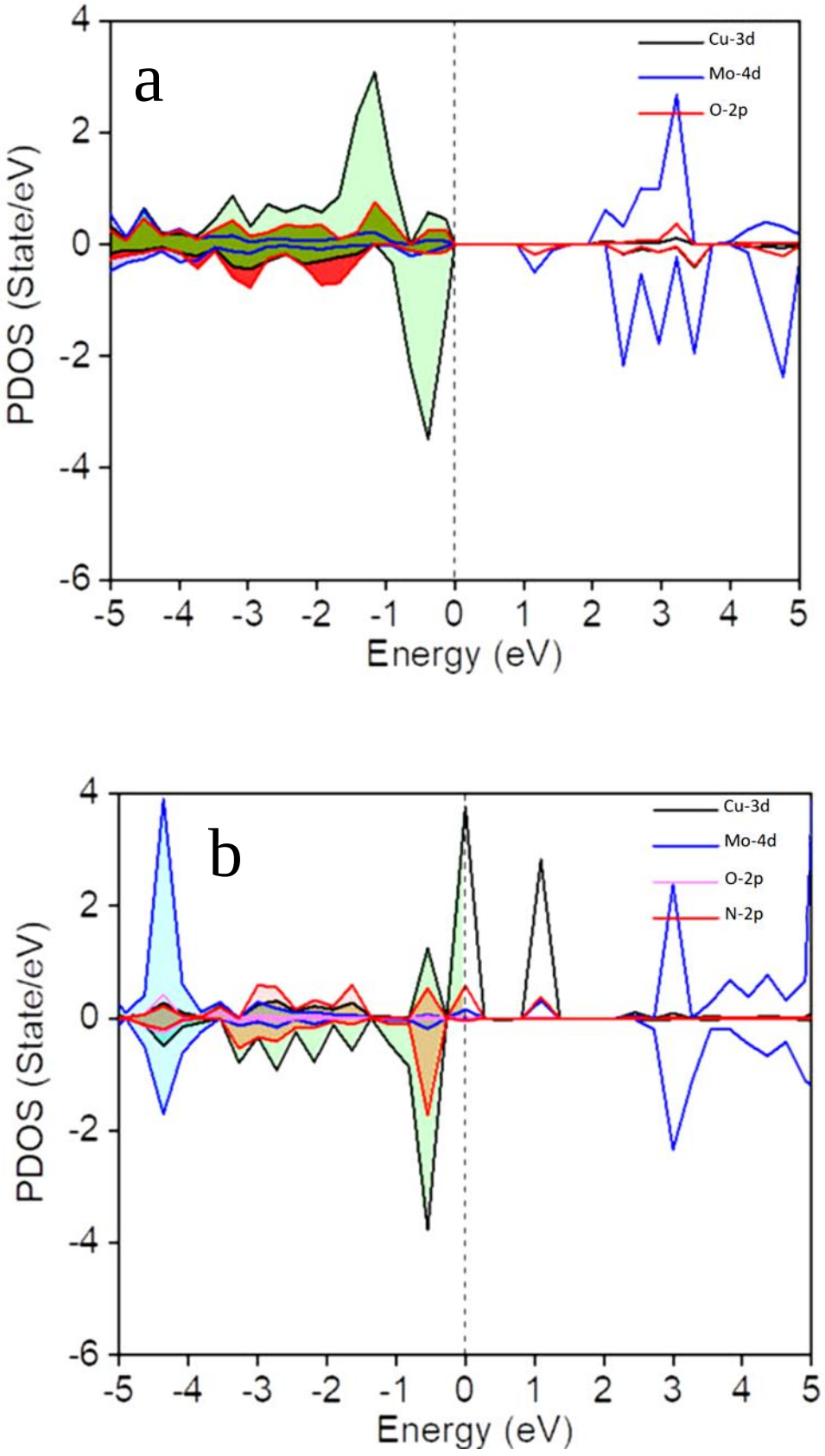


Figure 2.18: Partial density of sate (PDOS) of $Cu_3Mo_2O_9$ (002) (a) and (b) of N doped $Cu_3Mo_2O9$ (104) structure (b).

The spin-coupling partial density of state of doped and undoped $Cu_3Mo_2O_9$ was calculated to investigate electronic structure, as shown in Figure 2.18. In comparison with $Cu_3Mo_2O_9$, increased electronic states can be clearly observed in N-doped $Cu_3Mo_2O_9$, resulting in enhanced electron transfer and favored desorption/adsorption reaction mediates. It suggests that N in $Cu_3Mo_2O_9$ structure can cause modification of electronic configuration beneficial for HER and OER catalytic activities.

## 2.4 Conclusion

7N-Cu3Mo2O9 on NF is successfully synthesized in 2 steps: hydrothermal and calcination. Bifunctional catalyst possesses excellent electrochemically catalytic activity toward both HER and OER with good stability. Additionally, OWS also indicated that activity of 7N- $Cu_3Mo_2O_9$-baseelectrolyzeris noticeable when compare with commercial material Pt/C‖IrO2. To sum up, 7N-Cu3Mo2O9 can adapt the requirement of this research's purpose which has outstanding efficiency, good stability and lower cost when compare with commercial material in the same condition

# Chapter 3 Conclusions

Hydrogen energy is popular candidate for energy problem nowadays. Water splitting generating oxygen and Hydrogen fuel is attractive due to its potential to produce large amounts of green fuels. However, water splitting has draw back about relating to high energy barrier. Electrocatalyst is suitable solution in this issue. Traditionally, noble metal composites are often used in electrocatalyst. Although good electrochemical performance, this type of material is really expensive which is not adapt economics criterion of manufacturers. The demand of new generation catalyst increase. Electrocatalyst for water splitting requires good electrochemical performance, high stability and last but not least, the affordable price is attractive factors

Due to low cost and efficiency, transition metal is popularly studied for water splitting catalyst. However, the behavior of alloy is not as well as precious metal, it is necessity to optimize this potential material. The concept of morphology and electronic of composite is proven to highly impact OWS. Electronic structure optimization is recommended. Various reagents as metals, heteroatoms are tried and give outstanding results. Besides, adding different components also increase active site for the reaction in some cases. Furthermore, the surfactant is used in the process to control the morphology of composite. With suitable surfactant area, composite easily adsorb water and to desorb product.

This thesis orients to 2 aims:

(i) The research of water splitting and its catalyst especial HER catalyst. the theories of water splitting as principle, energy and catalyst are discussed

(ii) Optimize Copper Molybdenum for water splitting electrocatalyst. The second part describes the design and the synthesis of catalyst. Finally, the result is analyzed then the behavior of catalyst is explained

# References


1. Ebhota, W. S. & Jen, T. C. Fossil Fuels Environmental Challenges and the Role of Solar Photovoltaic Technology Advances in Fast Tracking Hybrid Renewable Energy System. *Int. J. Precis. Eng. Manuf. - Green Technol.*7, 97–117 (2020).

2. Basu, S. *et al.* Estimating US fossil fuel CO2 emissions from measurements of 14C in atmospheric CO2. *Proc. Natl. Acad. Sci. U. S. A.*117, 13300–13307 (2020).

3. Markewitz, D. Fossil fuel carbon emissions from silviculture: Impacts on net carbon sequestration in forests. *For. Ecol. Manage.*236, 153–161 (2006).

4. CO2 Emissions in 2022 – Analysis - IEA. https://www.iea.org/reports/co2-emissions-in-2022.

5. Rayner, P. J. *et al.* Journal of geophysical research. *Nature*175, 238 (1955).

6. Sharma, S., Agarwal, S. & Jain, A. Significance of hydrogen as economic and environmentally friendly fuel. *Energies*14, (2021).

7. Veziroğlu, T. N. & Şahin, S. 21st Century's energy: Hydrogen energy system. *Energy Convers. Manag.*49, 1820–1831 (2008).

8. Zhang, J., Zhang, Q. & Feng, X. Support and Interface Effects in Water-Splitting Electrocatalysts. *Adv. Mater.*31, 1–19 (2019).

9. Over, H. Fundamental Studies of Planar Single-Crystalline Oxide Model Electrodes (RuO2, IrO2) for Acidic Water Splitting. *ACS Catal.*11, 8848–8871 (2021).

10. Yu, Z. Y. *et al.* Clean and Affordable Hydrogen Fuel from Alkaline Water Splitting: Past, Recent Progress, and Future Prospects. *Adv. Mater.*33, (2021).

11. Zhang, X.-Y. *et al.* An overview of the active sites in transition metal electrocatalysts and their practical activity for hydrogen evolution reaction. *Chem. Eng. J.*430, 132312 (2022).

12. Wang, X. *et al.* Strategies for design of electrocatalysts for hydrogen evolution under alkaline

conditions. *Mater. Today*36, 125–138 (2020).

13. Quaino, P., Juarez, F., Santos, E. & Schmickler, W. Volcano plots in hydrogen electrocatalysis-uses and abuses. *Beilstein J. Nanotechnol.*5, 846–854 (2014).

14. Wei, J. *et al.* Heterostructured Electrocatalysts for Hydrogen Evolution Reaction Under Alkaline Conditions. *Nano-Micro Lett*10, 75 (2018).

15. Zhang, L., Fan, Q., Li, K., Zhang, S. & Ma, X. *First-row transition metal oxide oxygen evolution electrocatalysts: regulation strategies and mechanistic understandings*. *Sustainable Energy and Fuels* vol. 4 (2020).

16. Suen, N. T. *et al.* Electrocatalysis for the oxygen evolution reaction: Recent development and future perspectives. *Chem. Soc. Rev.*46, 337–365 (2017).

17. Jiao, Y., Yang, C., Wang, H., Zhong, Y. & Hu, Y. Optimization strategies on the advanced engineering of Co-based nanomaterials for electrochemical oxygen evolution. *J. Alloys Compd.*890, 161929 (2022).

18. Lee, Y., Suntivich, J., May, K. J., Perry, E. E. & Shao-Horn, Y. Synthesis and activities of rutile IrO 2 and RuO 2 nanoparticles for oxygen evolution in acid and alkaline solutions. *J. Phys. Chem. Lett.*3, 399–404 (2012).

19. Li, W., Wang, C. & Lu, X. Integrated transition metal and compounds with carbon nanomaterials for electrochemical water splitting. *J. Mater. Chem. A*9, 3786–3827 (2021).

20. Mandavkar, R. *et al.* Electron enriched ternary NiMoB electrocatalyst for improved overall water splitting: Better performance as compared to the Pt/C || RuO2 at high current density. *Appl. Mater. Today*29, 101579 (2022).

21. Wang, J. *et al.* Earth-abundant transition-metal-based bifunctional catalysts for overall electrochemical water splitting: A review. *J. Alloys Compd.*819, 153346 (2020).

22. Rajput, A., Kundu, A. & Chakraborty, B. Recent Progress on Copper-Based Electrode

Materials for Overall Water-Splitting. *ChemElectroChem*8, 1698–1722 (2021).

23. Li, X. P., Huang, C., Han, W. K., Ouyang, T. & Liu, Z. Q. Transition metal-based electrocatalysts for overall water splitting. *Chinese Chem. Lett.*32, 2597–2616 (2021).

24. You, B. & Sun, Y. Innovative Strategies for Electrocatalytic Water Splitting. *Acc. Chem. Res.*51, 1571–1580 (2018).

25. Marini, S. *et al.* Advanced alkaline water electrolysis. *Electrochim. Acta*82, 384–391 (2012).

26. Hu, C., Zhang, L. & Gong, J. Recent progress made in the mechanism comprehension and design of electrocatalysts for alkaline water splitting. *Energy Environ. Sci.*12, 2620–2645 (2019).

27. Audichon, T. *et al.* IrO2 Coated on RuO2 as Efficient and Stable Electroactive Nanocatalysts for Electrochemical Water Splitting. *J. Phys. Chem. C*120, 2562–2573 (2016).

28. Yoo, H. *et al.* Simultaneous co-doping of RuO2 and IrO2 into anodic TiO2 nanotubes: A binary catalyst for electrochemical water splitting. *Int. J. Hydrogen Energy*42, 6657–6664 (2017).

29. Luo, F. *et al.* Robust and Stable Acidic Overall Water Splitting on Ir Single Atoms. *Nano Lett.*20, 2120–2128 (2020).

30. Fang, Y. *et al.* In situ growth of graphdiyne based heterostructure: Toward efficient overall water splitting. *Nano Energy*59, 591–597 (2019).

31. Peng, X. *et al.* Recent progress of transition metal nitrides for efficient electrocatalytic water splitting. *Sustain. Energy Fuels*3, 366–381 (2019).

32. Balogun, M. S. *et al.* Updates on the development of nanostructured transition metal nitrides for electrochemical energy storage and water splitting. *Mater. Today*20, 425–451 (2017).

33. Luc, W., Jiang, Z., Chen, J. G. & Jiao, F. Role of Surface Oxophilicity in Copper-Catalyzed Water Dissociation. *ACS Catal.*8, 9327–9333 (2018).

34. Debbichi, L., Marco De Lucas, M. C., Pierson, J. F. & Krüger, P. Vibrational properties of CuO and Cu 4O 3 from first-principles calculations, and raman and infrared spectroscopy. *J. Phys. Chem. C*116, 10232–10237 (2012).

35. Saravanakumar, B., Ravi, G., Yuvakkumar, R., Ganesh, V. & Guduru, R. K. Synthesis of polyoxometalates, copper molybdate (Cu 3 Mo 2 O 9 ) nanopowders, for energy storage applications. *Mater. Sci. Semicond. Process.*93, 164–172 (2019).

36. Saravanakumar, B., Ravi, G., Yuvakkumar, R., Ganesh, V. & Guduru, R. K. Synthesis of polyoxometalates, copper molybdate (Cu 3 Mo 2 O 9 ) nanopowders, for energy storage applications. *Mater. Sci. Semicond. Process.*93, 164–172 (2019).

37. Ruan, D. *et al.* High-Performance Porous Molybdenum Oxynitride Based Fiber Supercapacitors. *ACS Appl. Mater. Interfaces*9, 29699–29706 (2017).

38. Qiu, J. *et al.* Supplementary Information Formation of N-doped molybdenum carbide confined into hierarchical and hollow carbon nitride microspheres with of Chemistry , Chemical Engineering and Environment of Foreign Languages , Liaoning Shihua University , Fushun ,. (2016).

39. Peng, C. *et al.* Lithiation-Enabled High-Density Nitrogen Vacancies Electrocatalyze CO2 to C2 Products. *Adv. Mater.*33, 1–7 (2021).

40. Mukhopadhyay, A. K. *et al.* Self-buckled effect of cubic Cu3N film: Surface stoichiometry. *AIP Conf. Proc.*1953, 1–5 (2018).

41. Schwarz, K. Band structure and chemical bonding in transition metal carbides and nitrides. *Crit. Rev. Solid State Mater. Sci.*13, 211–257 (1987).

42. Jamil, R. *et al.* The role of nitrogen in transition-metal nitrides in electrochemical water splitting. *Chem Catal.*1, 802–854 (2021).

43. Wei, W., Huang, W. F., Yang, Z., Guo, L. & Wu, Z. Y. Effect of the sheet thickness on the electrochemical performance of 2-D SnO2 nanomaterial as Li ion battery anode material. *Appl.*

*Mech. Mater.*472, 720–724 (2014).

44. Du, C.; Shang, M.; Mao, J.; Song, W. Hierarchical MoP/Ni2P heterostructures on nickel foam for efficient water splitting. J. Mater. Chem. A 2017, 5, 15940–15949.
45. Cui, S., Qian, M., Liu, X., Sun, Z., & Du, P. (2016). A Copper Porphyrin-Based Conjugated Mesoporous Polymer-Derived Bifunctional Electrocatalyst for Hydrogen and Oxygen Evolution. *ChemSusChem*, *9*(17), 2365–2373.
46. Yu, Z.-Y.; Duan, Y.; Gao, M.-R.; Lang, C.-C.; Zheng, Y.-R.; Yu, S.-H. A one-dimensional porous carbon-supported Ni/Mo2C dual catalyst for efficient water splitting. Chem. Sci. 2017, 8, 968–973.
47. Yin, Z.; Sun, Y.; Zhu, C.; Li, C.; Zhang, X.; Chen, Y.-J. Bimetallic Ni-Mo nitride nanotubes as highly active and stable bifunctional electrocatalysts for full water splitting. J. Mater. Chem. A 2017, 5, 13648–13658.
48. Pu, Z.; Wei, S.; Chen, Z.; Mu, S. Flexible molybdenum phosphide nanosheet array electrodes for hydrogen evolution reaction in a wide pH range. Appl. Catal. B 2016, 196, 193–198
49. Du, Z. Chen, S. Ye, B. J. Wiley, T. J. Meyer, *Angew. Chem. Int. Ed.* 2015, 54, 2073– 2078
50. Y. Sun, C. Wang, T. Ding, J. Zuo, Q. Yang, Fabrication of amorphus CoMoS4 as a bifunctional electrocatalyst for water splitting under strong alkline conditions, Nanoscale 8 (2016) 18887–18892.
51. P. Hu, Z. Jia, H. Che, W. Zhou, N. Liu, F. Li, J. Wang, Engineering hybrid CoMoS4/ Ni3S2 nanostructures as efficient bifunctional electrocatalyst for overall water splitting, J. Power Sources 416 (2019) 95–103, https://doi.org/10.1016/j. jpowsour.2019.01.090.
52. Yadav, A. A., Hunge, Y. M. & Kang, S. W. Ultrasound assisted synthesis of highly active nanoflower-like CoMoS4 electrocatalyst for oxygen and hydrogen evolution reactions. *Ultrason. Sonochem.* 72, 105454 (2021)
53. Sivanantham, A., Ganesan, P. & Shanmugam, S. Hierarchical NiCo2S4 Nanowire Arrays Supported on Ni Foam: An Efficient and Durable Bifunctional Electrocatalyst for Oxygen and Hydrogen Evolution Reactions. *Adv. Funct. Mater.* 26, 4661–4672 (2016).

54. W. Zhu, X. Yue, W. Zhang, S. Yu, Y. Zhang, J. Wang, J. Wang, Chem. Commun. 2016, 52, 1486.

55. J. Shi, J. Hu, Y. Luo, X. Sun, A. M. Asiri, Catal. Sci. Technol. 2015, 5, 4954